Energetic, exergetic and ecological (3E) evaluations of a hybrid system based on a phosphoric acid fuel cell and an organic Rankine cycle

Xinru Guo [a, c], Houcheng Zhang [a], Shujin Hou [b, *], Meng Ni [c], Tianjun Liao [c, d, *]

[a] *Department of Microelectronic Science and Engineering, Ningbo University, Ningbo 315211, China*

[b] *College of Physics and Electronic Engineering, Nanyang Normal University, Nanyang, Henan 47306, China*

[c] *Department of Building and Real Estate, The Hong Kong Polytechnic University, Hong Kong, China*

[d] *Department of Physics and Energy, Chongqing University of Technology, Chongqing 400054, China*

Abstract: The waste heat from phosphoric acid fuel cells (PAFCs) is available and suitable for additional power generation by means of organic Rankine cycles (ORCs). A new hybrid system model is proposed by integrating PAFC with ORC, where the ORC model is modified in absence of complex working fluid properties. The energetic, exergetic and ecological (3E) performances for the PAFC-ORC hybrid system are evaluated based on thermodynamic laws and steady-state mathematical models. Numerical results show that maximum power output density and maximum ecological objective function (EOF) density of the hybrid system are increased about 25.2 % and 57.5% by comparing to that of the single PAFC system, respectively. Optimum working regions of various performance parameters for the hybrid system are determined considering the trade-offs between multiple optimization criteria. Moreover, the effects of the operating temperature, exchange current density, electrolyte thickness and pinch temperature ratio on the hybrid system performance are analyzed. The obtained results may provide some help for understanding the 3E performance of such an actual cogeneration system.

Key Words: Phosphoric acid fuel cell; Organic Rankine cycle; Energetic; Exergetic; Ecological

* Corresponding authors.

Email addresses: houshujingrb@163.com (S. Hou); tianjun.liao@polyu.edu.hk (T. Liao).

1. Introduction

The depletion of fossil fuel reserves, ongoing energy crises and increasing pollution promote development of renewable energy sources [1, 2]. The fuel cell (FC) technologies have been considered as a solution to help humankind to resist global warming and meet energy demand, and they have attracted widespread attention, especially in some developed countries including US, UK, Japan and Korea [3, 4]. According to the data from the US Department of Energy [5], the FC market increased from $630 million in 2013 to about $2.54 billion in 2018, highlighting the growing interest and prospect of FCs.

Among a variety of FCs, phosphoric acid fuel cells (PAFCs) are considered to be one of the most commercialized and well-established hydrogen-oxygen fuel cell technologies [6, 7]. This is because PAFCs have high durability and simple structure due to their moderate operating temperature. However, some disadvantages still limit the further development of PAFCs, such as the low power density, short lifetime and high manufacturing cost [8]. In order to solve those problems, a number of previous works were focused on materials [9, 10], electrochemical techniques [11, 12], transport processes [13, 14], stack systems [15-17] and etc. [18, 19]. These results have laid solid foundations for the performance improvement and quickly accelerating the commercialization process.

In the last decade, relevant studies about PAFC-based hybrid systems have aimed to further improve the fuel utilization [20-25]. The waste heat produced by PAFCs can be harvested to drive some energy conversion devices for the combined cooling, heating, and power (CCHP) applications. The first commercial-scale combined heating and power (CHP) system for PAFC was introduced in 1970s [4]. Since then, the heat-driven refrigerator [20, 21] and thermoelectric cooler [7, 22] were

reported for additional cooling purposes. For additional power generation, Chen et al. [23] used the thermoelectric generator (TEG) to recover the waste heat from PAFC. Açıkkalp [24] evaluated a PAFC-TEG hybrid system with the economic and thermoeconomic point of views. In addition, Açıkkalp et al. [25] also proposed a thermally regenerative electrochemical cycle to recover the PAFC waste heat [25].

Organic Rankine cycles (ORCs) are widely used to recycle various low-grade heat energies, such as solar energy [26], biomass energy [27], geothermal heat [28, 29], industrial waste heat [30, 31], etc. [32]. The ORC performance is routinely related to the detailed working fluid properties. However, Zhao et al. [33] and Perna et al. [34] found that the impacts of working fluid properties on the ORC performance were negligible under optimal conditions. Moreover, Lee et al. [35, 36] developed analytical models to optimize the ORC performance without any working fluid data. It was discovered that the thermal efficiency at the ORC maximum power mainly was dependent on the initial temperatures and pinch-temperature differences of the heating and cooling fluids.

Due to the unique merits such as simple equipment, high security and efficiency, ORCs have been widely used as waste heat recovery technologies for fuel cells [33, 34, 37-45]. For example, Angelino et al. [37] and Vatani et al. [38] proposed molten carbonate fuel cell-ORC hybrid systems, and Mamaghani et al. [39] further studied the integrated system performance based on the energetic, exergetic, economic and environmental evaluations. Akkaya et al. [40] proposed an SOFC-ORC hybrid system and revealed the impacts of some representative operating parameters on the hybrid system performance. Al-Sulaiman et al. [41, 42] performed the energetic and exergetic analyses for this system, and then Pierobon et al. [43] further investigated the system performance using thermodynamic analyses. Furthermore, Borello et al. [44] and He et al. [45] conducted evaluations

on the performances of proton exchange membrane fuel cell (PEMFC)-ORC hybrid power systems. However, so far, performance evaluation on the PAFC-ORC hybrid system is seldom researched, which may provide valuable insights for the practical operation and optimum design of such a hybrid system.

In the present work, a PAFC-ORC hybrid system is proposed to evaluate its performance based on the 3E analyses. Each component within the hybrid system will be mathematically described in detail, where the ORC will adopt an optimization model without any input of working fluid properties. Mathematical expressions for power output, energetic efficiency, exergy destruction rate, exergetic efficiency, EOF and ecological coefficient of performance (ECOP) for the PAFC, ORC and PAFC-ORC hybrid system will be derived, from which the 3E performance characteristics for PAFC-ORC hybrid system will be evaluated. Optimum working regions of various performance parameters for the hybrid system will be also determined using different optimization criteria. Furthermore, the influences of some typical parameters on the 3E performances for the PAFC-ORC hybrid system will be discussed.

2. System description

The working principle of the PAFC-ORC hybrid system is schematically presented by Fig. 1. The hybrid system consists of a PAFC, an ORC and a regenerator, where the regenerator preheats the imported air and fuel using the high-temperature gas products out of the PAFC. The ORC consists of two heat exchangers (HEA and HEB), an expander (EX), a generator (GE), a condenser (CO) and a pump (PU). The PAFC acts as the high-temperature heat source that drives the ORC. In the PAFC, the electrochemical reaction produces electric power generation P_{fc} and waste heat. The produced electricity is transported to loads by an external circuit. A part of the waste heat, $\dot{Q}_L$, is dissipated

into the environment inevitably, meanwhile, the second part $\dot{Q}_{\mathrm{re}}$ is transferred to the regenerator to compensate the regeneration losses, and the third part $\dot{Q}_H$ is used to drive the ORC for the output power P_{orc}. $\dot{Q}_C$ is the heat rate from the ORC to the environment.

The following hypotheses are made to simplify the hybrid system model:

- Reactants of the fuel cell are completely consumed [46];
- The working temperature and pressure for the PAFC are constants [21];
- The PAFC-ORC hybrid system works at steady-state conditions [47];
- The cold and hot junction temperatures for the ORC are equal to the environment and PAFC working temperatures, respectively [23];
- Reactants of the PAFC are ideal gases that have constant thermodynamic and electrochemical properties [21];
- Factors leading to energy dissipation in the ORC are neglected [36];
- The ORC is worked under optimization states.

2.1. Phosphoric acid fuel cell

The PAFC is composed of an anode, a cathode and an electrolyte, which works as the topping cycle of the hybrid system. The chemical energies of hydrogen and oxygen are directly converted into electrical and thermal energies in the PAFC. The overall fuel cell reaction inside the PAFC can be expressed as: $\mathrm{H_2(g)+1/2O_2(g)\rightarrow H_2O(g)+electricity+heat}$. The fuel cell theoretical maximum potential, i.e., named reversible potential, can be derived by the Nernst equation [47], i.e.,

$$U_{rev}=\frac{\Delta g^0}{n_e F}+\frac{RT}{n_e F}\ln\left(\frac{a_{\mathrm{H_2}}a_{\mathrm{O_2}}^{0.5}}{a_{\mathrm{H_2O}}}\right) \tag{1}$$

where Δg^0 is the change of molar Gibbs free energy of the electrochemical reaction under standard conditions, and $n_e=2$ is the number of electrons transferred per hydrogen molecule [7]; F and

R are, respectively, the Faraday's constant and universal gas constant; $a_{\mathrm{H_2}}$, $a_{\mathrm{O_2}}$ and $a_{\mathrm{H_2O}}$ are, respectively, the partial pressures of $\mathrm{H_2}$, $\mathrm{O_2}$ and $\mathrm{H_2O}$ [23]. Due to the ohmic overpotential (U_{ohm}), concentration overpotential (U_{con}) and activation overpotential (U_{act}), the output voltage of the PAFC U_{fc} is smaller than U_{rev}, which can be explicitly given by [23]

$$U_{fc} = U_{rev} - U_{ohm} - U_{con} - U_{act} \tag{2}$$

$$U_{ohm} = \frac{t_{ele}}{\kappa} j \tag{3}$$

$$U_{con} = b\exp(cj) \tag{4}$$

$$U_{act} = \frac{RT}{\alpha n_e F}\ln\left(\frac{j}{j_0}\right) \tag{5}$$

where j is the operating current density of the PAFC; t_{ele} is the electrolyte thickness; κ is the specific conductivity for the aqueous phosphoric acid solution [25]; b and c are two constants that can be found in Ref. [7]; α and j_0 are, respectively, the charge transfer coefficient and exchange current density [25].

The power output, P_{fc}, and electric efficiency, η_{fc}, for the PAFC are, respectively, given by [23, 48]

$$P_{fc} = U_{fc} jA = \left[U_{rev} - \frac{RT}{an_e F}\ln\left(\frac{j}{j_0}\right) - b\exp(cj) - \frac{t_{ele}}{\kappa} j\right] jA \tag{6}$$

and

$$\eta_{fc} = \frac{P_{fc}}{-\Delta \dot{H}} \tag{7}$$

where $-\Delta \dot{H} = -\frac{jA\Delta h}{n_e F}$ stands for the total energy released by the reaction per unit time; A is the electrode effective surface area; and Δh is the change of the molar enthalpy [7].

The exergy destruction rate, ExD_{fc}, and exergetic efficiency, φ_{fc}, for the PAFC can be,

respectively, given by [47]

$$ExD_{fc} = -\Delta \dot{G} - T\Delta \dot{S}\left(1 - T_0/T\right) - P_{fc} \tag{8}$$

and

$$\varphi_{fc} = \frac{P_{fc}}{-\Delta \dot{G} - T\Delta \dot{S}\left(1 - T_0/T\right)} \tag{9}$$

where $-\Delta \dot{G} = -\frac{jA\Delta g}{n_e F}$ and $-\Delta \dot{S} = -\frac{jA\Delta s}{n_e F}$ are, respectively, the total Gibbs free energy change rate and the total entropy change rate [46]; Δg is the molar Gibbs free energy change; and Δs stands for the molar entropy change.

The entropy production rate for the PAFC, $\dot{\delta}_{fc}$, can be calculated as [49, 50]

$$\dot{\delta}_{fc} = (-\Delta \dot{H} - P_{fc})/T \tag{10}$$

The EOF for the PAFC, E_{fc}, can be defined as [49]

$$E_{fc} = P_{fc} - T_0 \dot{\delta}_{fc} \tag{11}$$

The ECOP for the PAFC, ϕ_{fc}, can be expressed as [49]

$$\phi_{fc} = P_{fc}/(T_0 \dot{\delta}_{fc}) \tag{12}$$

2.2. Regenerator

Based on Refs. [23, 33], the regeneration loss rate is directly proportional to the temperature difference between exhaust products and inlet reactants, i.e.,

$$\dot{Q}_{re} = K_{re} A_{re}\left(1 - \beta\right)\left(T - T_0\right) \tag{13}$$

where K_{re} is the heat-transfer coefficient of the regenerator; A_{re} and β are, respectively, the heat-transfer area and effectiveness.

2.3. Organic Rankine cycle

As shown in Fig. 1, the ORC operates between the hot reservoir (i.e., PAFC) and the cold

reservoir (i.e., environment). The HEB of the ORC can increase the temperature of the subcooled liquid from the PU by a relatively high-temperature liquid from the EX. The ORC adopts a modified Rankine engine model, which is alternately connected to cooling fluid and heating fluid with finite-rate heat capacities [51]. The temperature-entropy (*T*-*S*) diagram for the modified ORC is shown in Fig. 2, and the modified ORC can be equivalently regarded as a Carnot cycle operating between temperatures T_e and T_c [36]. The ORC includes four processes: isobaric heating (4-1), adiabatic expansion (1-2), isobaric exothermic (2-3) and adiabatic compression (3-4). Due to the low efficiencies of the EX and PU, the expansion and compression processes are non-isentropic and can be described as 1-2′ and 3-4′, respectively. The heat source temperature initially cools from T_{H1} to T_{H2} with the heat rejection, and the heat sink temperature initially warms up from T_{L1} to T_{L2} with the heat addition. Thus, the heat input rate $\dot{Q}_H$ and heat rejection rate $\dot{Q}_L$ of the ORC can be, respectively, computed as [35]

$$\dot{Q}_H = C_H (T_{H1} - T_{H2}) \tag{14}$$

$$\dot{Q}_L = C_L (T_{L2} - T_{L1}) \tag{15}$$

The outlet temperatures of heating fluid at HEA and cooling fluid at HEB are, respectively, given by [36]

$$T_{H2} = T_e + T_{PH} \tag{16}$$

$$T_{L2} = T_c + T_{PL} \tag{17}$$

Combining Eqs. (14) - (17), one has

$$\dot{Q}_H = C_H (T_{He} - T_e) \tag{18}$$

$$\dot{Q}_L = C_L (T_c - T_{Le}) \tag{19}$$

where C_H and C_L are, respectively, the heat capacities for the heating fluid and cooling fluid, and

$$T_{He} = T_{H1} - T_{pH} \tag{20}$$

$$T_{Le} = T_{L1} - T_{pL} \tag{21}$$

T_{pH} and T_{pL} are the pinch temperatures for the heating fluid and cooling fluid [36].

Based on the second law of thermodynamics, the entropy generation rate of the ORC can be expressed as [51]

$$\dot{\delta}_{orc} = \dot{Q}_L / T_c - \dot{Q}_H / T_e \tag{22}$$

Based on Eqs. (18) and (19), Eq. (22) can be rewritten as

$$\dot{\delta}_{orc} = \frac{C_L (T_c - T_{Le})}{T_c} - \frac{C_H (T_{He} - T_e)}{T_e} \tag{23}$$

Thus, T_e can be given by

$$T_e = \frac{C_L T_{He} T_c}{C_l (T_c - T_{Le}) + C_H T_c - T \dot{\delta}_{orc}} \tag{24}$$

According to Eqs. (18), (19) and (24), the output power for the ORC, P_{orc}, can be calculated as [36]

$$P_{orc} = \dot{Q}_H - \dot{Q}_L = C_H \left[T_{He} - \frac{C_L T_{He} T_c}{C_l (T_c - T_{Le}) + C_H T_c - T_c \dot{\delta}_{orc}} \right] - C_L (T_c - T_{Le}) \tag{25}$$

Substituting Eq. (25) into the extreme condition $\partial P_{orc} / \partial T_e = 0$, one has

$$T_c = T_{Le}^{0.5} \frac{C_H T_{He}^{0.5} + C_L T_{Le}^{0.5}}{C_H + C_L - \dot{\delta}_{orc}} \tag{26}$$

Thus, P_{orc} can be rewritten as

$$P_{orc} = \frac{x(1-x) C_T^2 \left(T_{He}^{0.5} - T_{Le}^{0.5} \right)^2 - C_T \left(x T_{He} - (1-x) T_{Le} \right) \dot{\delta}_{orc}}{C_T - \dot{\delta}_{orc}} \tag{27}$$

where $x = C_H / C_T$ and $C_T = C_H + C_L$.

Substituting Eq. (27) into the extreme condition $\partial P_{orc} / \partial x = 0$, one has

$$x_{opt} = 0.5 - 0.5\frac{\left(T_{He}^{0.5} + T_{Le}^{0.5}\right)\dot{\delta}_{orc}}{\left(T_{He}^{0.5} - T_{Le}^{0.5}\right)C_T} \tag{28}$$

The output power of the ORC can be rewritten as

$$P_{orc} = \frac{x_{opt}\left(1\text{-}x_{opt}\right)C_T^2\left(T_{He}^{0.5} - T_{Le}^{0.5}\right)^2 - C_T\left(x_{opt}T_{He} - \left(1 - x_{opt}\right)T_{Le}\right)\dot{\delta}_{orc}}{C_T - \dot{\delta}_{orc}} \tag{29}$$

The energy efficiency for the ORC, η_{orc}, can be defined as [23]

$$\eta_{orc} = P_{orc} / \dot{Q}_H \tag{30}$$

The exergy destruction rate for the ORC, ExD_{orc}, can be given by [47]

$$ExD_{orc} = \dot{Q}_H\left(1 - T_0/T_H\right) - \dot{Q}_L\left(1 - T_0/T_L\right) + P_{orc} \tag{31}$$

The exergetic efficiency of the ORC, φ_{orc}, can be written as [49]

$$\varphi_{orc} = \frac{P_{orc}}{\dot{Q}_H\left(1 - T_0/T_H\right)} \tag{32}$$

The EOF for the ORC, E_{orc}, can be given by [49]

$$E_{orc} = P_{orc} - T_0\dot{\delta}_{orc} \tag{33}$$

The ECOP for the ORC, ϕ_{orc}, can be expressed as [49]

$$\phi_{orc} = P_{orc} / (T_0\dot{\delta}_{orc}) \tag{34}$$

2.4. Performance of the hybrid system

According to the Newton's heat-transfer law and the first law of thermodynamics, $\dot{Q}_L$ and $\dot{Q}_H$ can be, respectively, given by [47, 52]

$$\dot{Q}_L = \alpha_L A_L (T - T_0) \tag{35}$$

and

$$\dot{Q}_H = -\Delta\dot{H} - P_{fc} - \dot{Q}_{re} - \dot{Q}_L = A\left[\left(1 - \eta_{\mathrm{FC}}\right)\frac{-\Delta h}{n_e F}j - \left(c_1 + c_2\right)\left(T - T_0\right)\right] \tag{36}$$

where α_L and A_L are the heat-leak coefficient and the heat-leak area, respectively; $c_1=[K_{re}A_{re}(1-\beta)]/A$ and $c_2=(\alpha_L A_L)/A$ are two temperature independent constants related to the heat transfer irreversibilities, effectiveness of the regenerator, geometric size of the regenerator and the PAFC and polar plate area of the PAFC [20]. Combining Eqs. (18) and (36), the heat capacity of the heating fluid for the ORC can be further expressed as

$$C_H=\frac{A}{T_{He}-T_e}\left[(1-\eta_{\mathrm{FC}})\,j\frac{-\Delta h}{n_e F}-(c_1+c_2)(T-T_0)\right] \tag{37}$$

The power output, P_{hy}, and energy efficiency, η_{hy}, of the hybrid system can be, respectively, written as

$$P_{hy}=P_{fc}+P_{orc} \tag{38}$$

and

$$\eta_{hy}=P_{hy}/(-\Delta \dot{H}) \tag{39}$$

The output power for the ORC P_{orc} can be equivalently described by an output voltage $U_{orc,eq}$ with respect to the PAFC operating electric current [36], and thus one has

$$U_{orc,eq}=P_{orc}/Aj \tag{40}$$

Therefore, the equivalent output voltage for the hybrid system $U_{hy,eq}$ can be given by [36]

$$U_{hy,eq}=P_{hy}/Aj=U_{fc}+U_{orc,eq} \tag{41}$$

The exergy destruction rate, ExD_{hy}, and exergetic efficiency, φ_{hy}, for the hybrid system can be, respectively, expressed as [41]

$$ExD_{hy}=-\Delta \dot{G}-T\Delta \dot{S}(1-T_0/T)-P_{hy} \tag{42}$$

and

$$\varphi_{hy}=\frac{P_{hy}}{-\Delta \dot{G}-T\Delta \dot{S}(1-T_0/T)} \tag{43}$$

The entropy production rate for the hybrid system, $\dot{\delta}_{hy}$, can be given by

$$\dot{\delta}_{hy} = (-\Delta \dot{H} - P_{hy}) / T \tag{44}$$

The EOF for the hybrid system, E_{hy}, can be calculated by [49]

$$E_{hy} = P_{hy} - T_0 \dot{\delta}_{hy} \tag{45}$$

The ECOP for the hybrid system, ϕ_{hy}, can be given by [49]

$$\phi_{hy} = \frac{P_{hy}}{T_0 \dot{\delta}_{hy}} \tag{46}$$

The energy efficiency for the ORC, $\eta_{orc,eq}$, can be determined as [36]

$$\eta_{orc,eq} = \frac{P_{orc}}{-\Delta \dot{H}} \tag{47}$$

The equivalent exergetic efficiency, $\varphi_{orc,eq}$, and the equivalent ECOP, $\phi_{orc,eq}$, for the ORC in term of the hybrid system can be, respectively, described as [36]

$$\varphi_{orc,eq} = \frac{P_{orc}}{-\Delta \dot{G} - T \Delta \dot{S} \left(1 - T_0 / T\right)} \tag{48}$$

and

$$\phi_{orc,eq} = P_{orc} / (T_0 \dot{\delta}) \tag{49}$$

3. Results and discussion

On the basis of default parameters in Table 1, the 3E performance characteristics for the PAFC-ORC hybrid system can be evaluated. These parameters are considered as unchanged ones unless specified elsewhere.

3.1. Generic performance characteristics

The current-voltage curves for the PAFC, ORC and hybrid system are shown in Fig. 3. The operating voltage for the PAFC, U_{fc}, decreases with j due to the increases of U_{ohm}, U_{act} and U_{con} as j increases. The equivalent voltage for the ORC, $U_{orc,eq}$, monotonically increases with j

because the heat rate from the PAFC to the ORC increases with j. However, the total equivalent voltage of the hybrid system, $U_{hy,eq}$, is a monotonically decreasing function of j, because the reduction of U_{fc} is larger than the increment of $U_{orc,eq}$ as j increases.

Figs. 4~6 compare the 3E performances between the PAFC system, ORC and hybrid system, respectively, where $P_{fc}^{*} = P_{fc} / A$, $P_{orc}^{*} = P_{orc} / A$ and $P_{hy}^{*} = P_{hy} / A$ are the power densities for the single PAFC system, ORC and hybrid system, respectively; $ExD_{fc}^{*} = ExD_{fc} / A$ ($E_{fc}^{*} = E_{fc} / A$), $ExD_{orc}^{*} = ExD_{orc} / A$ ($E_{orc}^{*} = E_{orc} / A$) and $ExD_{hy}^{*} = ExD_{hy} / A$ ($E_{hy}^{*} = E_{hy} / A$) are the corresponding exergy destruction rate densities (EOF densities), respectively; P_{orc}^{*}, $\eta_{orc,eq}$, ExD_{fc}^{*}, ExD_{orc}^{*}, ExD_{hy}^{*}, $\varphi_{orc,eq}$, E_{orc}^{*} and $\phi_{orc,eq}$ are monotonically increasing functions of j, while η_{fc}, η_{hy}, φ_{fc}, φ_{hy}, ϕ_{fc} and ϕ_{hy} are monotonically decreasing functions of j. P_{fc}^{*}, P_{hy}^{*}, E_{fc}^{*} and E_{hy}^{*} first ascend and then descend with j, while they attain maximum values at different j. Through numerical calculation, a maximum power density of $P_{hy,\max}^{*}$=6036.7 W m^{-2} and a corresponding optimal current density of $j_{hy,P} = 9470.8$ A m^{-2} of the hybrid system can be achieved. Comparing to the maximum power density $P_{fc,\max}^{*}$=4822.4 W m^{-2} and the corresponding optimal current density $j_{fc,P} = 8760.8$ A m^{-2} of the single PAFC system, it is found that the maximum power density and optimal current density of hybrid system are larger than those of the single PAFC system. E_{hy}^{*} attains its maximum $E_{hy,\max}^{*}$, 2913.1 W m^{-2}, at $j = j_{hy,E} = 7050.8$ A m^{-2}, while E_{fc}^{*} reaches its maximum $E_{fc,\max}^{*}$, 1850.0 W m^{-2}, at $j = j_{fc,E} = 5270.8$ A m^{-2}. $E_{hy,\max}^{*}$ is approximately 57.5% higher than $E_{fc,\max}^{*}$. $\eta_{hy.P}$ ($\eta_{fc.P}$), $ExD_{hy,P}^{*}$ ($ExD_{fc,P}^{*}$), $\varphi_{hy,P}$ ($\varphi_{fc,P}$), $E_{hy,P}^{*}$ ($E_{fc,P}^{*}$) and $\phi_{hy,P}$ ($\phi_{fc,P}$) are the energy efficiency, exergy destruction rate density, exergetic efficiency, EOF density and ECOP for the hybrid system (single PAFC system) at $j = j_{hy,P}$ ($j = j_{fc,P}$). $P_{hy,E}^{*}$ ($P_{fc,E}^{*}$), $\eta_{hy.E}$ ($\eta_{fc.E}$), $ExD_{hy,E}^{*}$ ($ExD_{fc,E}^{*}$), $\varphi_{hy,E}$ ($\varphi_{fc,E}$) and $\phi_{hy,E}$ ($\phi_{fc,E}$) are the output power density, energy

efficiency, exergy destruction rate density, exergetic efficiency and ECOP for the hybrid system (single PAFC system) at $j = j_{hy,E}$ ($j = j_{fc,E}$). For the typical parameters given in Table 1, the above key performance parameters are compared in Table 2. It can be seen from Table 2 that the 3E performances of the hybrid system are significantly better than those of a single PAFC system in terms of either output power optimization criterion or EOF optimization criterion. From the above analyses, coupling an ORC to a PAFC is an effective way for performance improvement.

To obtain the optimal working regions, the variations of the exergetic efficiency (curves 1 and 2) and EOF density (curves 3, 4 and 5) for the hybrid system with power density are illustrated in Fig. 7, where $\varphi_{hy,\max}$ is the maximum of φ_{hy}. φ_{hy} increases at the expense of P_{hy}^* in the curve 1, while it decreases as P_{hy}^* reduces in the curve 2. By considering the balance between energetic and exergetic performances, the optimal regions for the PAFC-ORC hybrid system should be $0 \le j \le j_{hy,P}$, $0 \le P_{hy}^* \le P_{hy,\max}^*$, $\varphi_{hy,\max} \le \varphi_{hy} \le \varphi_{hy,P}$ and $0 \le E_{hy}^* \le E_{hy,P}^*$. On the other hand, E_{hy}^* improves as P_{hy}^* arises in curves 3 and 5, while it increases at the expense of P_{hy}^* in the curve 4. By considering the trade-off between energetic and ecological performances, the optimal regions for the PAFC-ORC hybrid system should be located in $j_{hy,E} \le j \le j_{hy,P}$, $P_{hy,E}^* \le P_{hy}^* \le P_{hy,\max}^*$, $\varphi_{hy,P} \le \varphi_{hy} \le \varphi_{hy,E}$ and $E_{hy,P}^* \le E_{hy}^* \le E_{hy,\max}^*$.

4. Parametric study

To further understand the thermodynamic performance of the PAFC-ORC hybrid system, in this section, the effects of some key parameters (including the operating temperature, exchange current density, electrolyte thickness and pinch temperature ratio) on 3E performances for the hybrid system are discussed through parametric studies.

4.1. Effects of operating temperature

Fig. 8 shows the 3E performances under different operating temperatures T. An increasing T can simultaneously enhance the gas effective diffusion, electrochemical reactivity and ionic conductivity of the PAFC as well as the power output and energy efficiency of the ORC. Thus, the performance of the PAFC-ORC hybrid system is improved with the increasing T. Fig. 8 also illustrates that P_{hy}^{*}, η_{hy}, φ_{hy}, E_{hy}^{*} and ϕ_{hy} increase while ExD_{hy}^{*} diminishes as T increases. $P_{hy,\max}^{*}$ is equal to 5640.9, 6036.7 and 6300.9 W m^{-2} and $E_{hy,\max}^{*}$ is equal to 2509.0, 2913.1 and 3242.0 W m^{-2} when T is set as 433, 453 and 473 K, respectively. In Fig. 9, $j_{hy,P}$, $P_{hy,\max}^{*}$, $\varphi_{hy,P}$, $E_{hy,P}^{*}$, $j_{hy,E}$, $P_{hy,E}^{*}$ and $E_{hy,\max}^{*}$ are improved with the increase of T, while $\varphi_{hy,E}$ is reduced as T raises. Although a larger T is beneficial for improving the hybrid system performance, it may also cause some problems such as worse stability, longer start-up time and shut-down time.

4.2. Effects of electrolyte thickness

Fig. 10 shows the 3E performances for the hybrid system under different electrolyte thicknesses t_{ele}. It can be seen from Eq. (3) that t_{ele} has a positive influence on the ohmic overpotential U_{ohm}. Therefore, the performances of the PAFC system and the hybrid system can be turned by adjusting the thicknesses t_{ele}. As verified in Fig. 10, the 3E performances of the hybrid system are improved while P_{hy}^{*}, η_{hy}, φ_{hy}, E_{hy}^{*} and ϕ_{hy} are decreased as t_{ele} is decreased. For the typical parameters in Table 1, when t_{ele} is equal to 0.001, 0.002 and 0.003 m, $P_{hy,\max}^{*}$ are 7325.9, 6036.7 and 4905.5 W m^{-2} and $E_{hy,\max}^{*}$ are 4323.6, 2913.1 and 2066.1 W m^{-2}, respectively. Furthermore, $j_{hy,P}$, $P_{hy,\max}^{*}$, $\varphi_{hy,P}$, $E_{hy,P}^{*}$, $j_{hy,E}$, $P_{hy,E}^{*}$, $\varphi_{hy,E}$ and $E_{hy,\max}^{*}$ are reduced as t_{ele} increases. As a result, decreasing the electrolyte thickness can improve the hybrid system performances. Simultaneously, the mechanical properties of the electrolyte are somewhat reduced as the electrolyte thickness descends [53].

4.3. Effects of exchange current density

The exchange current density j_0 is the rate for both oxidation and reduction per unit of electrode area at equilibrium states. It is a measure of the ability for the electrode to perform an electrochemical reaction [54, 55]. A higher j_0 means that the surface of the electrode is more active. Thus the activation overpotential U_{act} is a monotonically decreasing function of j_0 as shown in Eq. (5), and a larger j_0 is beneficial for exergetic and ecological performances of the PAFC-ORC hybrid system. As shown in Fig. 11, $j_{hy,P}$, $P^*_{hy,\max}$, $\varphi_{hy,P}$, $E^*_{hy,P}$, $j_{hy,E}$, $P^*_{hy,E}$, $\varphi_{hy,E}$ and $E^*_{hy,\max}$ are increased with an increase in j_0. Moreover, P^*_{hy}, η_{hy}, φ_{hy}, E^*_{hy} and ϕ_{hy} are improved while ExD^*_{hy} is diminished as j_0 increases. When j_0 is 0.02, 0.06 and 0.1 A m^{-2}, $P^*_{hy,\max}$ equals 5801.2, 6036.7 and 6146.7 W m^{-2} and $E^*_{hy,\max}$ is 2626.6, 2913.1 and 3049.9 W m^{-2}, respectively. So far, researchers are trying to increase the phosphoric acid concentration, operating temperature, electrode catalyst loading, catalyst specific surface area and so on to improve the exchange current density of the fuel cell [55].

4.4. Effects of pinch temperature ratio

$\gamma = T_{pL}/T_{pH}$ is defined as the pinch temperature ratio which affects the ORC performance. Based on Eqs. (18)-(21), the output power for the ORC can be given by

$$\begin{aligned} P_{orc} &= C_H(T_{H1} - T_{pH} - T_e) - C_L(T_c - T_{L1} + T_{pL}) \\ &= C_H\left[(T_{H1} - T_e) - \left(\frac{1}{x_{opt}} - 1\right)(T_c - T_{L1} + T_M) + \left(\frac{1}{x_{opt}} - 2\right)\frac{T_M}{1+\gamma}\right] \end{aligned} \tag{50}$$

where $T_M = T_{pL} + T_{pH}$. Based on Eq. (28), one has $x_{opt} < 0.5$, i.e., $\left(x_{opt}^{-1} - 2\right) > 0$, and thus P_{orc} decreases as γ increases. Thus, the PAFC-ORC hybrid system performances are degraded with γ, as displayed in Fig. 12. P^*_{hy}, η_{hy}, φ_{hy}, E^*_{hy} and ϕ_{hy} are diminished while ExD^*_{hy} is improved as γ increases. $P^*_{hy,\max}$ is equal to 6138.7, 6036.7 and 5989.0 W m^{-2} and $E^*_{hy,\max}$ is equal to 3015.6,

2913.1 and 2866.8 W m^{-2} when γ is fixed as 1/3, 1, 3, respectively. In Fig. 13, $j_{hy,P}$, $P^*_{hy,\max}$, $\varphi_{hy,P}$, $E^*_{hy,P}$, $j_{hy,E}$, $P^*_{hy,E}$, $\varphi_{hy,E}$ and $E^*_{hy,\max}$ are decreased as γ increases.

5. Conclusions

A theoretical model of PAFC-ORC hybrid system has been established with the aim to harvest the waste heat from the PAFC for additional electricity generation via ORC. Mathematical expressions for the power, energy efficiency, exergy destruction rate, exergetic efficiency, EOF and ECOP for the stand-alone PAFC, ORC and PAFC-ORC hybrid system are derived, from which the 3E performances for PAFC-ORC hybrid system are revealed. The maximum power density for the hybrid system ($P^*_{hy,\max}$=6036.7 W m^{-2}) allows approximately 25.2% higher than that of the single PAFC system ($P^*_{fc,\max}$=4822.4 W m^{-2}). The maximum EOF density for the hybrid system (E^*_{hy}=2913.1 W m^{-2}) allows approximately 57.5% higher than that of the single PAFC system ($E^*_{fc,\max}$=1850.0 W m^{-2}). ORCs are found to be effective for waste heat recovery for PAFCs. The optimal working regions for various performance parameters are determined using different optimization criteria. Furthermore, the effects for various parameters on the 3E performances of the PAFC-ORC hybrid system are revealed. The obtained research results may provide some new insights and valuable guidance for PAFC performance improvement via cogeneration approaches.

Acknowledgments

This work has been supported by the Natural Science Foundation of Zhejiang Province (Grant No. LY20E060002), the Science and Technology Research Program of Chongqing Municipal Education Commission (Grant No. KJQN201901144), and the K. C. Wong Magna Fund in Ningbo University, China.

Nomenclature

A	Effective polar plate area of PAFC (m^2)
A_L	Heat-transfer area between the fuel cell and the environment (m^2)
a	Partial pressures (atm)
b	Constant in Eq. (4)
C	Heat capacity rate (W)
c	Constant in Eq. (4)
c_1 and c_2	Constants in Eq. (36) (W m^{-2} K^{-1})
E	Ecological objective function (W)
ExD	Exergy destruction rate (W)
F	Faraday's constant (C mol^{-1})
$-\Delta G$	Gibbs free energy change (J)
$-\Delta H$	Total energies released (J)
j	Operating current density of the PAFC (A m^{-2})
j_0	Exchange current density of the PAFC (A m^{-2})
K_L	Heat-leak coefficient (W m^{-2} K^{-1})
n_e	Number of electrons exchanged per hydrogen molecule
U	Voltage (V)
U_{act}	Activation overpotential (V)
U_{con}	Concentration overpotential (V)
U_{ohm}	Ohmic overpotential (V)
U_{rev}	Reversible potential (V)

P	Power output (W)
Q	Heat (J)
R	Universal gas constant (J mol^{-1} K^{-1})
$-\Delta S$	Entropy change ($J K^{-1}$)
T	Operating temperature of PAFC (K)
t_{ele}	Thickness of the electrolyte (cm)
x	Heat capacity rate
Greek symbols	
α	Charge transfer coefficient
β	Regenerator effectiveness
δ	Entropy production ($J K^{-1}$)
ϕ	Ecological coefficient of performance
φ	Exergetic efficiency
η	Electric efficiency
σ_{ele}	Proton conductivity of the electrolyte (Ωm^{-1})
ε	Irreversibility ratio of the ORC
γ	Pinch temperature ratio
Subscripts	
0	Ideal standard
eq	Equivalent
fc	Phosphoric acid fuel cell
H	High

hy	PAFC-ORC hybrid system
L	Low
max	Maximum
orc	Organic Rankine cycle
p	Pinch
re	Regenerative
*	Unit area
Δ	Difference
•	Unit time

References

[1] Karvonen M, Kapoor R, Uusitalo A, Ojanen V. Technology competition in the internal combustion engine waste heat recovery: a patent landscape analysis. Journal of Cleaner Production 2016; 112: 3735-3743.

[2] Wu Z, Zhu P, Yao J, Tan P, Xu H, Chen B, Yang F, Zhang Z, Ni M. Thermo-economic modeling and analysis of an NG-fueled SOFC-WGS-TSA-PEMFC hybrid energy conversion system for stationary electricity power generation. Energy 2019: 116613.

[3] Xu Q, Zhang F, Xu L, Leung P, Yang C, Li H, Ekins P. The applications and prospect of fuel cells in medical field: a review. Renewable and Sustainable Energy Reviews 2017; 67: 574-580.

[4] Di Marcoberardino G, Binotti M, Manzolini G, Lores M, Upham P, Dütschke E, Schneider U, Schneider P. Achievements of European projects on membrane reactor for hydrogen production. Journal of Cleaner Production 2017; 161: 1442-1450.

[5] http://www.fuelcelltoday.com/analysis.

[6] Ito H. Economic and environmental assessment of phosphoric acid fuel cell-based combined heat and power system for an apartment complex. International Journal of Hydrogen Energy 2017; 42: 15449-15463.

[7] Wu M, Zhang H, Zhao J, Yuan J. Performance analyzes of an integrated phosphoric acid fuel cell and thermoelectric device system for power and cooling cogeneration. International Journal of Refrigeration 2018; 89: 61-69.

[8] Wang S, Jiang S P. Prospects of fuel cell technologies. National Science Review 2017; 4: 163-166.

[9] Lu C L, Chang C P, Guo Y H, Yeh T K, Su Y C, Wang P C. High-performance and low-leakage

phosphoric acid fuel cell with synergic composite membrane stacking of micro glass microfiber and nano PTFE. Renewable Energy 2019; 134: 982-988.

[10] Strickland K, Pavlicek R, Miner E, Jia Q, Zoller I, Ghoshal S, Liang W, Mukerjee S. Anion resistant oxygen reduction electrocatalyst in phosphoric acid fuel cell. Acs Catalysis 2018; 8: 3833-3843.

[11] Eapen D E, Suseendiran S R, Rengaswamy R. Phosphoric acid fuel cells. Woodhead Publishing 2016; 57-70.

[12] Odetola P, Popoola P, Popoola O, Delport D. Electrodeposition of Functional Coatings on Bipolar Plates for Fuel Cell Applications–A Review. Electrodeposition of Composite Materials 2016; 231.

[13] Paul T, Banerjee D, Kargupta K. Conductivity of phosphoric acid: an in situ comparative study of proton in phosphoric acid fuel cell. Ionics 2015; 21: 2583-2590.

[14] Strickland K, Pavlicek R, Miner E, Jia Q, Zoller I, Ghoshal S. Anion resistant oxygen reduction electrocatalyst in phosphoric acid fuel cell. Acs Catalysis 2018; 8: 3833-3843.

[15] Wang H S, Chang C P, Huang Y J, Su Y C, Tseng F G. A high-yield and ultra-low-temperature methanol reformer integratable with phosphoric acid fuel cell (PAFC). Energy 2017; 133: 1142-1152.

[16] Pachauri R K, Chauhan Y K. Various control schemes of power management for phosphoric acid fuel cell system. International Journal of Electrical Power & Energy Systems 2016; 74: 49-57.

[17] Abdul-Aziz A, Alkasab K A. Performance of serpentine passages in the cooling system of a phosphoric acid fuel cell stack. Experimental Thermal and Fluid Science 1994; 8: 101-111.

[18] Choudhury S R, Deshmukh M B, Rengaswamy R. A two-dimensional steady-state model for

phosphoric acid fuel cells (PAFC). Journal of Power Sources 2002; 112: 137-152.

[19] Zervas P L, Koukou M K, Markatos N C. Predicting the effects of process parameters on the performance of phosphoric acid fuel cells using a 3-D numerical approach. Energy Conversion and Management 2006; 47: 2883-2899.

[20] Chen X, Wang Y, Zhao Y, Zhou Y. A study of double functions and load matching of a phosphoric acid fuel cell/heat-driven refrigerator hybrid system. Energy 2016; 101: 359-365.

[21] Yang P, Zhang H, Hu Z. Parametric study of a hybrid system integrating a phosphoric acid fuel cell with an absorption refrigerator for cooling purposes. International Journal of Hydrogen Energy 2016; 41: 3579-3590.

[22] Kwan T H, Yao Q. Exergetic and temperature analysis of a fuel cell-thermoelectric device hybrid system for the combined heat and power application. Energy Conversion and Management 2018; 173: 1-14.

[23] Chen X, Wang Y, Cai L, Zhou Y. Maximum power output and load matching of a phosphoric acid fuel cell-thermoelectric generator hybrid system. Journal of Power Sources 2015; 294: 430-436.

[24] Açıkkalp E. Performance assessment of phosphoric acid fuel cell – thermoelectric generator hybrid system with economic aspect. Journal of Thermal Engineering 2019; 5: 29-45.

[25] Açıkkalp E, Ahmadi M H. Parametric investigation of phosphoric acid fuel cell-Thermally regenerative electro chemical hybrid system. Journal of Cleaner Production 2018; 203: 585-600.

[26] Ghorbani B, Mehrpooya M, Aasadnia M, Niasar M S. Hydrogen liquefaction process using solar energy and organic Rankine cycle power system. Journal of Cleaner Production 2019; 235: 1465-1482.

[27] Uusitalo A, Uusitalo V, Grönman A, Luoranen M, Jaatinen-Värri A. Greenhouse gas reduction

potential by producing electricity from biogas engine waste heat using organic Rankine cycle. Journal of Cleaner Production 2016; 127: 399-405.

[28] Astolfi M, Xodo L, Romano M C, Macchi E. Technical and economical analysis of a solar–geothermal hybrid plant based on an organic Rankine Cycle. Geothermics 2011; 40: 58-68.

[29] Hettiarachchi H D M, Golubovic M, Worek W M, Ikegami Y. Optimum design criteria for an organic Rankine cycle using low-temperature geothermal heat sources. Energy 2007; 32: 1698-1706.

[30] Larjola J. Electricity from industrial waste heat using high-speed organic Rankine cycle (ORC). InternationalJournal of Production Economics 1995; 41: 227-235.

[31] Hung T C, Shai T Y, Wang S K. A review of organic Rankine cycles (ORCs) for the recovery of low-grade waste heat. Energy 1997; 22: 661-667.

[32] Liu X, Liang J, Xiang D, Yang S, Qian Y. A proposed coal-to-methanol process with CO2 capture combined Organic Rankine Cycle (ORC) for waste heat recovery. Journal of Cleaner Production 2016; 129: 53-64.

[33] Zhao P, Wang J, Gao L, Dai Y. Parametric analysis of a hybrid power system using organic Rankine cycle to recover waste heat from proton exchange membrane fuel cell. International Journal of Hydrogen Energy 2012; 37: 3382-3391.

[34] Perna A, Minutillo M, Jannelli E. Investigations on an advanced power system based on a high temperature polymer electrolyte membrane fuel cell and an organic Rankine cycle for heating and power production. Energy 2015; 88: 874-884.

[35] Lee W Y, Kim S S, Won S H. Finite-time optimizations of a heat engine. Energy 1990; 15: 979-985.

[36] Lee W Y, Kim M, Sohn Y J, Kim S G. Power optimization of a combined power system

consisting of a high-temperature polymer electrolyte fuel cell and an organic Rankine cycle system. Energy 2016; 113: 1062-1070.

[37] Angelino G, di Paliano P C. Organic Rankine cycles (ORCs) for energy recovery from molten carbonate fuel cells. IEEE 2000; 2: 1400-1409.

[38] Vatani A, Khazaeli A, Roshandel R, Panjeshahi M H. Thermodynamic analysis of application of organic Rankine cycle for heat recovery from an integrated DIR-MCFC with pre-reformer. Energy Conversion and Management 2013; 67: 197-207.

[39] Mamaghani A H, Najafi B, Shirazi A, Rinaldi F. 4E analysis and multi-objective optimization of an integrated MCFC (molten carbonate fuel cell) and ORC (organic Rankine cycle) system. Energy 2015; 82: 650-663.

[40] Akkaya A V, Sahin B. A study on performance of solid oxide fuel cell - organic Rankine cycle combined system. International Journal of Energy Research 2009; 33: 553-564.

[41] Al-Sulaiman F A, Dincer I, Hamdullahpur F. Exergy analysis of an integrated solid oxide fuel cell and organic Rankine cycle for cooling, heating and power production. Journal of Power Sources 2010; 195: 2346-2354.

[42] Al-Sulaiman F A, Dincer I, Hamdullahpur F. Energy analysis of a trigeneration plant based on solid oxide fuel cell and organic Rankine cycle. International Journal of Hydrogen Energy 2010; 35: 5104-5113.

[43] Pierobon L, Rokni M, Larsen U, Haglind F. Thermodynamic analysis of an integrated gasification solid oxide fuel cell plant combined with an organic Rankine cycle. Renewable Energy 2013; 60: 226-234.

[44] Borello D, Del Prete Z, Marchegiani A, Rispoli F, Tortora E. Analysis of an integrated

PEMFC/ORC power system using ammonia for hydrogen storage. American Society of Mechanical Engineers Digital Collection 2012; 143-153.

[45] He T, Shi R, Peng J, Zhuge W, Zhang Y. Waste heat recovery of a PEMFC system by using organic Rankine cycle. Energies 2016; 9: 267.

[46] Guo X, Zhang H, Zhao J, Wang F, Wang J, Miao H, Yuan J. Performance evaluation of an integrated high-temperature proton exchange membrane fuel cell and absorption cycle system for power and heating/cooling cogeneration. Energy Conversion and Management 2019; 181: 292-301.

[47] Guo X, Zhang H, Yuan J, Wang J, Zhao J, Wang F, Miao H, Hou S. Energetic and exergetic analyses of a combined system consisting of a high-temperature polymer electrolyte membrane fuel cell and a thermoelectric generator with Thomson effect. International Journal of Hydrogen Energy 2019; 44: 16918-16932.

[48] Zhang H, Kong W, Dong F, Xu H, Chen B, Ni M. Application of cascading thermoelectric generator and cooler for waste heat recovery from solid oxide fuel cells. Energy Conversion and Management 2017; 148: 1382-1390.

[49] Angulo-Brown F. An ecological optimization criterion for finite-time heat engines. Journal of Applied Physics 1991; 69: 7465-9.

[50] Seifert U. Entropy production along a stochastic trajectory and an integral fluctuation theorem. Physical Review Letters 2005; 95: 040602.

[51] Lee W Y, Kim S S. Finite time optimization of a Rankine heat engine. Energy Conversion and Management 1992; 33: 59-67.

[52] Zhang H, Wang J, Wang F, Zhao J, Miao H, Yuan J. Performance assessment of an advanced triple-cycle system based upon solid oxide fuel cells, vacuum thermionic generators and absorption

refrigerators. Energy Conversion and Management 2019; 193: 64-73.

[53] Lu K. Materials in energy conversion, harvesting, and storage. John Wiley & Sons 2014.

[54] Mamlouk M, Scott K. A boron phosphate-phosphoric acid composite membrane for medium temperature proton exchange membrane fuel cells. Journal of Power Sources 2015; 286: 290-298.

[55] O'hayre R, Cha S W, Colella W, Prinz FB. Fuel cell fundamentals. John Wiley & Sons 2016.

Table captions

Table 1. Parameters used in the modeling.

Table 2. Performance parameter comparisons between the single PAFC system and the PAFC-ORC hybrid system.

Figure captions

Fig. 1. The schematic diagram of the PAFC-ORC hybrid system, where the ORC consists of two heat exchangers (HEA and HEB), an expander (EX), a generator (GE), a condenser (CO) and a pump (PU).

Fig. 2. Temperature-entropy diagram for the modified ORC.

Fig. 3. Current-voltage curves for the single PAFC system, ORC and PAFC-ORC hybrid system.

Fig. 4. Energetic performance comparisons between the single PAFC system, ORC and PAFC-ORC hybrid system: (a) power density; (b) energy efficiency, where $P_{fc}^{*} = P_{fc} / A$, $P_{orc}^{*} = P_{orc} / A$ and $P_{hy}^{*} = P_{hy} / A$ are the corresponding power densities; $P_{hy.\max}^{*}$ (at $j = j_{hy,P}$) and $P_{fc.amx}^{*}$ (at $j = j_{fc,P}$) are the maximum values for P_{hy}^{*} and P_{fc}^{*}, respectively; the maximum EOF densities for the hybrid system and the single PAFC system are obtained at $j = j_{hy,E}$ and $j = j_{fc,E}$; $P_{hy,E}^{*}$ ($P_{fc,E}^{*}$) is the value for P_{hy}^{*} (P_{fc}^{*}) at $j = j_{hy,E}$ ($j = j_{fc,E}$). $\eta_{fc.P}$ and $\eta_{fc.E}$ are, respectively, values of η_{fc} at $j = j_{fc,P}$ and $j = j_{fc,E}$, and $\eta_{hy.P}$ and $\eta_{hy.E}$ are values of η_{hy} at $j = j_{hy,P}$ and $j = j_{hy,E}$, respectively.

Fig. 5. Exergetic performance comparisons between the single PAFC system, ORC and PAFC-ORC hybrid system: (a) exergy destruction rate density; (b) exergetic efficiency, where $ExD_{fc}^{*} = ExD_{fc} / A$, $ExD_{orc}^{*} = ExD_{orc} / A$ and $ExD_{hy}^{*} = ExD_{hy} / A$ are the corresponding exergy destruction rate densities; $ExD_{hy.P}^{*}$ and $ExD_{hy.E}^{*}$ are, respectively, values for ExD_{hy}^{*} at $j = j_{hy,P}$ and at $j = j_{hy,E}$, $ExD_{fc.P}^{*}$ and $ExD_{fc.E}^{*}$ are, respectively, values for ExD_{fc}^{*} at

$j = j_{fc,P}$ and at $j = j_{fc,E}$; $\varphi_{hy.P}$ and $\varphi_{hy.E}$ are, respectively, values of φ_{hy} at $j = j_{hy,P}$ and $j = j_{hy,E}$; and $\varphi_{fc.P}$ and $\varphi_{fc.E}$ are values of φ_{fc} at $j = j_{fc,P}$ and $j = j_{fc,E}$, respectively.

Fig. 6. Ecological performance comparisons between the single PAFC system, the ORC and the PAFC-ORC hybrid system: (a) EOF density; (b) ECOP, where $E^*_{fc} = E_{fc} / A$, $E^*_{orc} = E_{orc} / A$ and $E^*_{hy} = E_{hy} / A$ are the corresponding EOF densities; $E^*_{hy.\max}$ and $E^*_{fc.amx}$ are, respectively, the maximum values for E^*_{hy} and E^*_{fc}; $E^*_{hy.P}$ and $E^*_{hy.E}$ are, respectively, values for E^*_{hy} at $j = j_{hy,P}$ and at $j = j_{hy,E}$, $E^*_{fc.P}$ and $E^*_{fc.E}$ are, respectively, values for E^*_{fc} at $j = j_{fc,P}$ and at $j = j_{fc,E}$; $\phi_{hy.P}$ and $\phi_{hy.E}$ are, respectively, values of ϕ_{hy} at $j = j_{hy,P}$ and $j = j_{hy,E}$; and $\phi_{fc.P}$ and $\phi_{fc.E}$ are values of ϕ_{fc} at $j = j_{fc,P}$ and $j = j_{fc,E}$, respectively.

Fig. 7. Variations of φ_{hy} (curves 1 and 2) and E^*_{hy} (curves 3, 4 and 5) versus P^*_{hy}.

Fig. 8. Effects of the operating temperature T on (a) energetic, (b) exergetic and (c) ecological performances for the PAFC-ORC hybrid system.

Fig. 9. (a) Variations of $j_{hy,P}$, $P^*_{hy,\max}$, $\varphi_{hy,P}$ and $E^*_{hy,P}$ versus T; and (b) Curves of $j_{hy,E}$, $P^*_{hy,E}$, $\varphi_{hy,E}$ and $E^*_{hy,\max}$ versus the operating temperature T.

Fig. 10. Effects of the electrolyte thickness t_{ele} on (a) energetic, (b) exergetic and (c) ecological performances for the PAFC-ORC hybrid system.

Fig. 11. Effects of the exchange current density j_0 on (a) energetic, (b) exergetic and (c) ecological performances for the PAFC-ORC hybrid system.

Fig. 12. Effects of the pinch temperature ratio γ on (a) energetic, (b) exergetic and (c) ecological performances for the PAFC-ORC hybrid system.

Fig. 13. (a) Variations of $j_{hy,P}$, $P^*_{hy,\max}$, $\varphi_{hy,P}$ and $E^*_{hy,P}$ versus the pinch temperature ratio γ; and (b) Curves of $j_{hy,E}$, $P^*_{hy,E}$, $\varphi_{hy,E}$ and $E^*_{hy,\max}$ versus the pinch temperature ratio γ.

Table 1. Parameters used in the modeling.

Parameter	Value
Faraday constant, F (C mol^{-1})	96,485
Universal gas constant, R (J mol^{-1} K^{-1})	8.314
Number of electrons, n_e	2 [7]
Operating pressure, p (atm)	1.0 [25]
Operating temperature, T (K)	453 [7]
Ambient temperature, T_0 (K)	298 [20]
Constant b	0.00003 [7]
Constant c	0.0008 [7]
Partial pressure of H_2, a_{H_2} (atm)	1.0 [23]
Partial pressure of O_2, a_{O_2} (atm)	0.105 [23]
Partial pressure of H_2O, a_{H_2O} (atm)	0.5 [23]
Charge transfer coefficient, α	0.5 [25]
Exchange current density, j_0 (A m^{-2})	0.06 [25]
Thickness of the electrolyte, t_{ele} (m)	0.002 [25]
Polar plate area of the cell, A (m^2)	0.0015 [7]
Constant, c_1 (W K^{-1} m^{-2})	0.2 [20]
Constant, c_2 (W K^{-1} m^{-2})	0.2 [20]
Pinch temperatures, T_{pH}, T_{pL} (K)	10, 10 [36]
Irreversibility ratio, ε	0.0075 [36]

Table 2. Performance parameter comparisons between the single PAFC system and the PAFC-ORC hybrid system.

	$\eta_{i,P}$ (%)	$ExD^{*}_{i,P}$ (W m^{-2})	$\varphi_{i,P}$ (%)	$E^{*}_{i,P}$ (W m^{-2})	$\phi_{i,P}$ (%)	$P^{*}_{i,E}$ (W m^{-2})	$\eta_{i,E}$ (%)	$ExD^{*}_{i,E}$ (W m^{-2})	$\varphi_{i,E}$ (%)	$\phi_{i,E}$ (%)
$i = fc$	43.7	7645.2	44.2	727.1	1.2	3758.3	56.5	3435.0	57.3	2.0
$i = hy$	50.5	5196.0	51.4	2151.3	1.5	5285.3	59.4	3077.1	60.3	2.2
Increase rate (%)	15.6	32.0	16.3	195.9	25	40.6	5.1	10.4	5.1	10

Fig. 1.

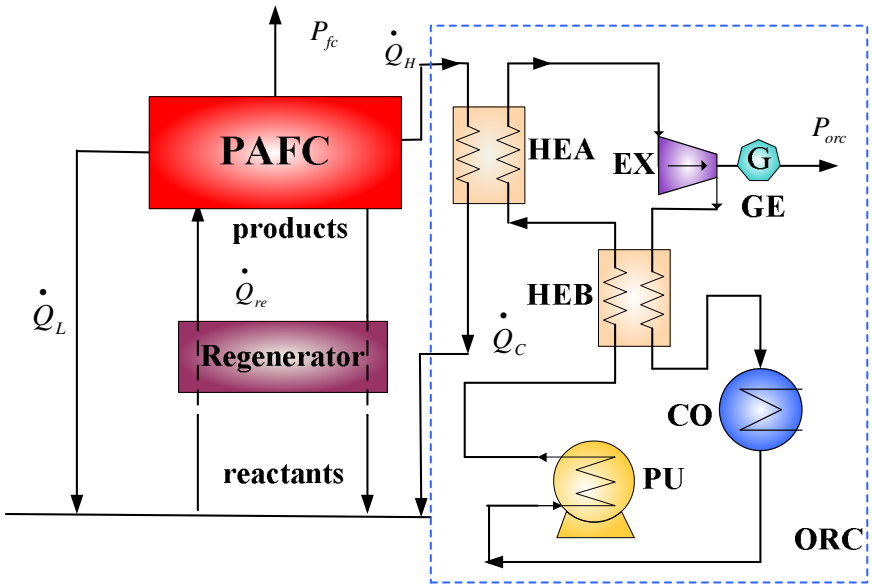

Fig. 1. The schematic diagram of the PAFC-ORC hybrid system, where the ORC consists of two heat exchangers (HEA and HEB), an expander (EX), a generator (GE), a condenser (CO) and a pump (PU).

Fig. 2.

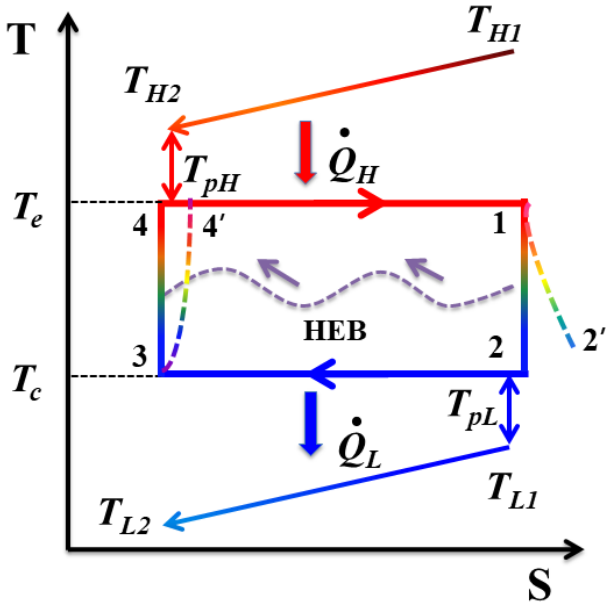

Fig. 2. Temperature-entropy diagram for the modified ORC.

Fig. 3.

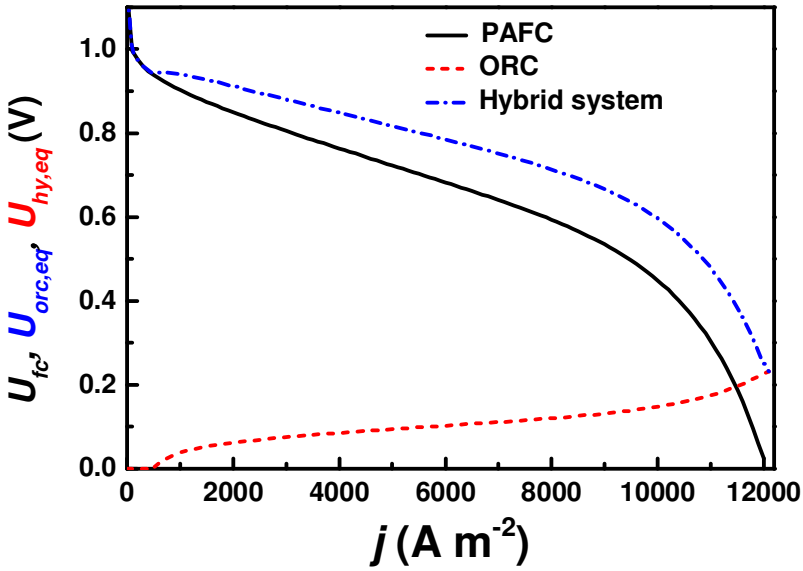

Fig. 3. Current-voltage curves for the single PAFC system, ORC and PAFC-ORC hybrid system.

Fig. 4.

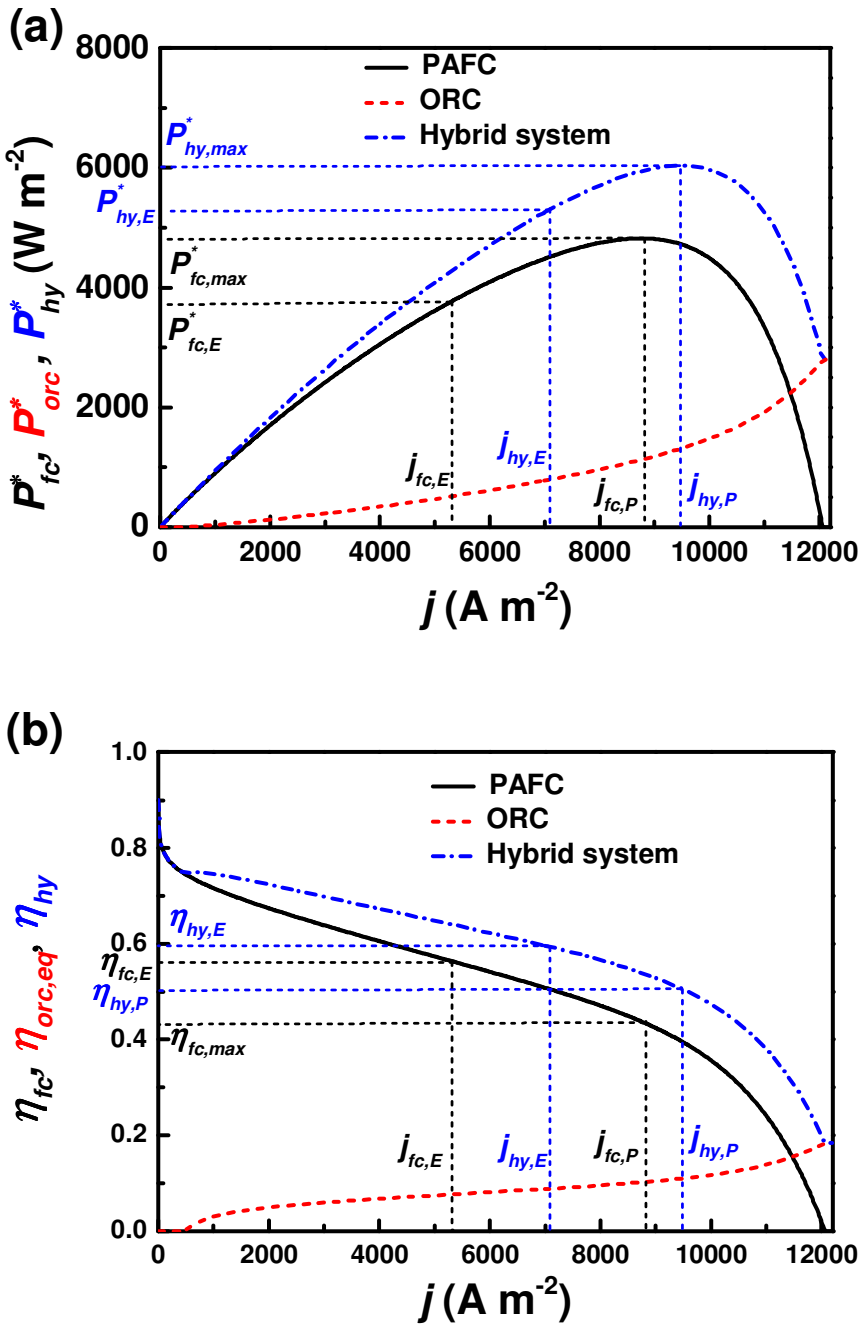

Fig. 4. Energetic performance comparisons between the single PAFC system, ORC and PAFC-ORC hybrid system: (a) power density; (b) energy efficiency, where $P^*_{fc} = P_{fc} / A$, $P^*_{orc} = P_{orc} / A$ and $P^*_{hy} = P_{hy} / A$ are the corresponding power densities; $P^*_{hy.\max}$ (at $j = j_{hy,P}$) and $P^*_{fc.amx}$

(at $j = j_{fc,P}$) are the maximum values for P_{hy}^{*} and P_{fc}^{*}, respectively; the maximum EOF densities for the hybrid system and the single PAFC system are obtained at $j = j_{hy,E}$ and $j = j_{fc,E}$; $P_{hy,E}^{*}$ ($P_{fc,E}^{*}$) is the value for P_{hy}^{*} (P_{fc}^{*}) at $j = j_{hy,E}$ ($j = j_{fc,E}$). $\eta_{fc.P}$ and $\eta_{fc.E}$ are, respectively, values of η_{fc} at $j = j_{fc,P}$ and $j = j_{fc,E}$, and $\eta_{hy.P}$ and $\eta_{hy.E}$ are values of η_{hy} at $j = j_{hy,P}$ and $j = j_{hy,E}$, respectively.

Fig. 5.

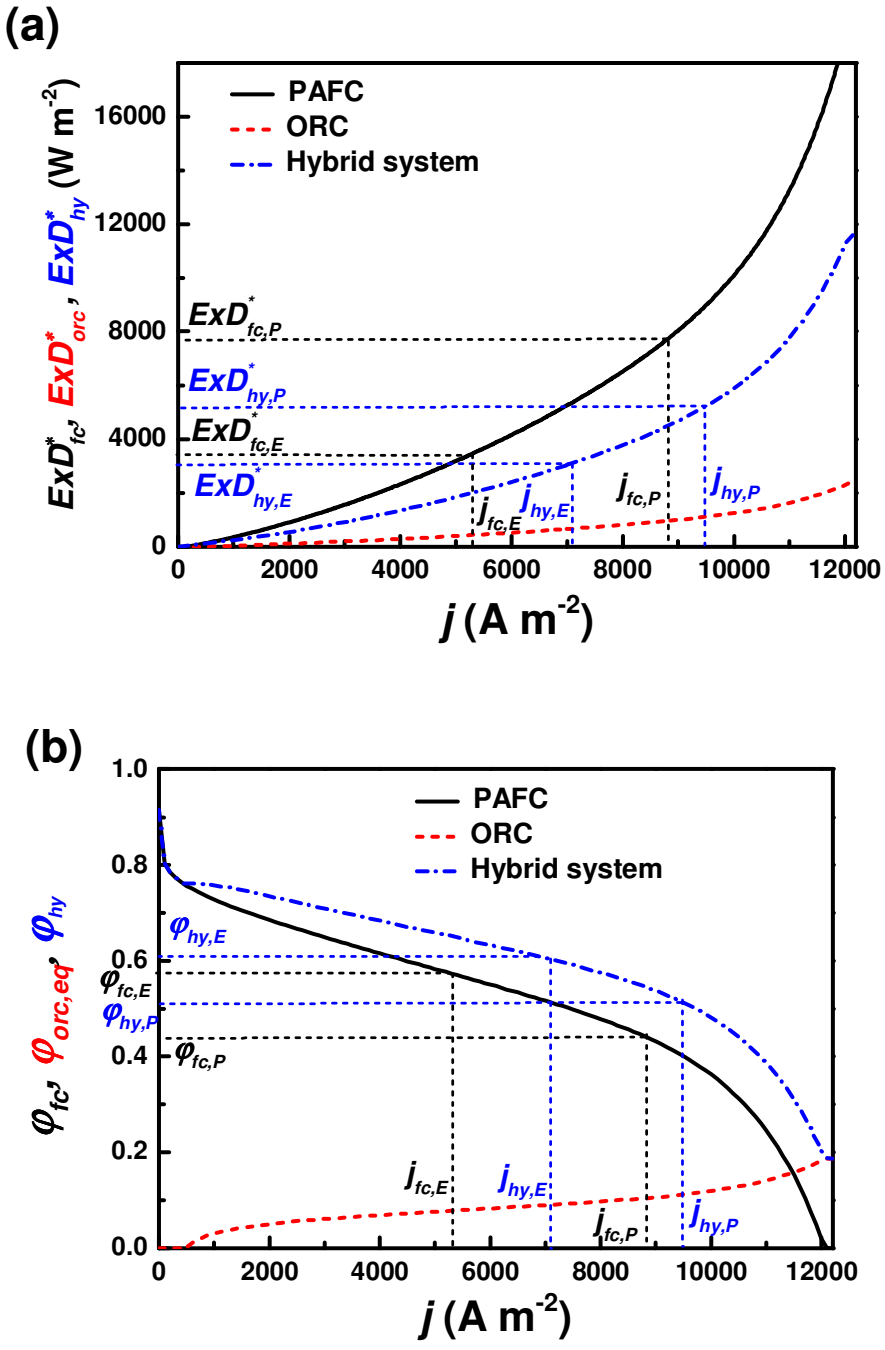

Fig. 5. Exergetic performance comparisons between the single PAFC system, ORC and PAFC-ORC hybrid system: (a) exergy destruction rate density; (b) exergetic efficiency, where $ExD^*_{fc} = ExD_{fc} / A$, $ExD^*_{orc} = ExD_{orc} / A$ and $ExD^*_{hy} = ExD_{hy} / A$ are the corresponding

exergy destruction rate densities; $ExD^*_{hy.P}$ and $ExD^*_{hy.E}$ are, respectively, values for ExD^*_{hy} at $j = j_{hy,P}$ and at $j = j_{hy,E}$, $ExD^*_{fc.P}$ and $ExD^*_{fc.E}$ are, respectively, values for ExD^*_{fc} at $j = j_{fc,P}$ and at $j = j_{fc,E}$; $\varphi_{hy.P}$ and $\varphi_{hy.E}$ are, respectively, values of φ_{hy} at $j = j_{hy,P}$ and $j = j_{hy,E}$; and $\varphi_{fc.P}$ and $\varphi_{fc.E}$ are values of φ_{fc} at $j = j_{fc,P}$ and $j = j_{fc,E}$, respectively.

Fig. 6.

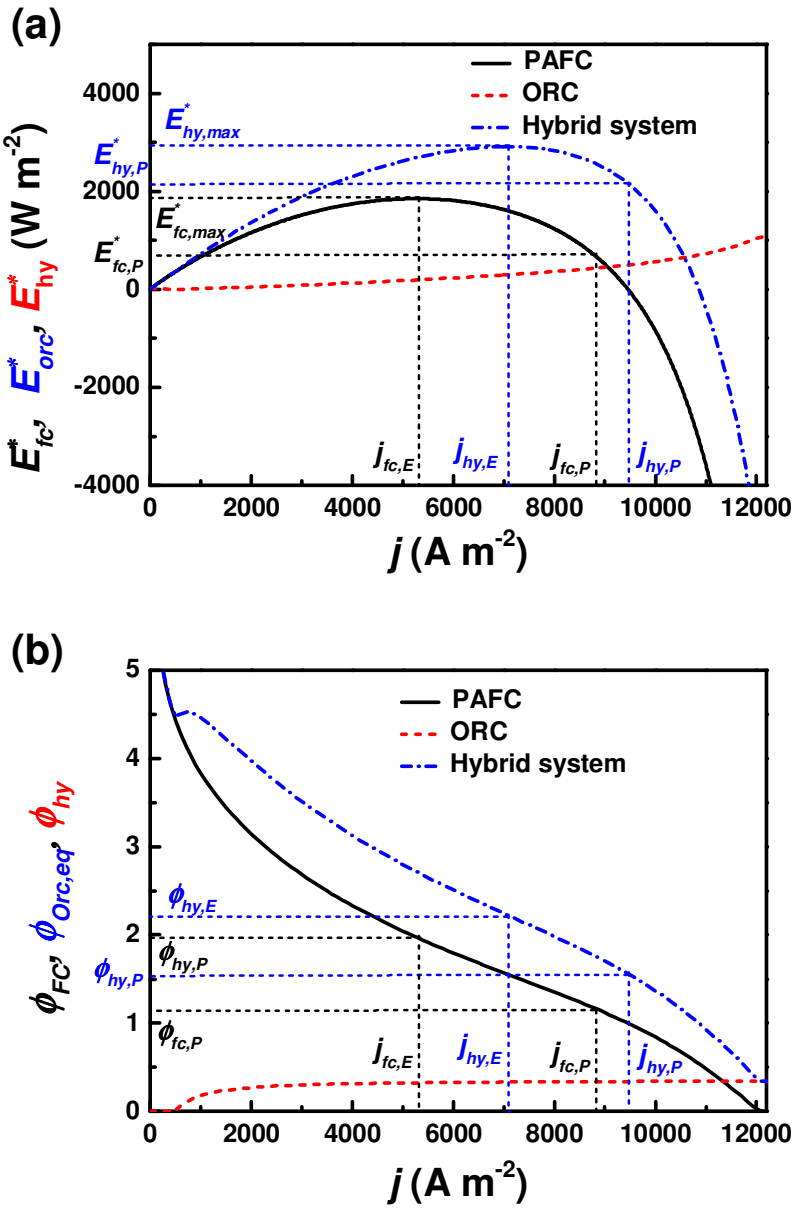

Fig. 6. Ecological performance comparisons between the single PAFC system, the ORC and the PAFC-ORC hybrid system: (a) EOF density; (b) ECOP, where $E^*_{fc} = E_{fc} / A$, $E^*_{orc} = E_{orc} / A$ and $E^*_{hy} = E_{hy} / A$ are the corresponding EOF densities; $E^*_{hy.\max}$ and $E^*_{fc.amx}$ are, respectively, the maximum values for E^*_{hy} and E^*_{fc}; $E^*_{hy.P}$ and $E^*_{hy.E}$ are, respectively, values for E^*_{hy} at $j = j_{hy,P}$ and at $j = j_{hy,E}$, $E^*_{fc.P}$ and $E^*_{fc.E}$ are, respectively, values for

E_{fc}^{*} at $j = j_{fc,P}$ and at $j = j_{fc,E}$; $\phi_{hy.P}$ and $\phi_{hy.E}$ are, respectively, values of ϕ_{hy} at $j = j_{hy,P}$ and $j = j_{hy,E}$; and $\phi_{fc.P}$ and $\phi_{fc.E}$ are values of ϕ_{fc} at $j = j_{fc,P}$ and $j = j_{fc,E}$, respectively.

Fig. 7.

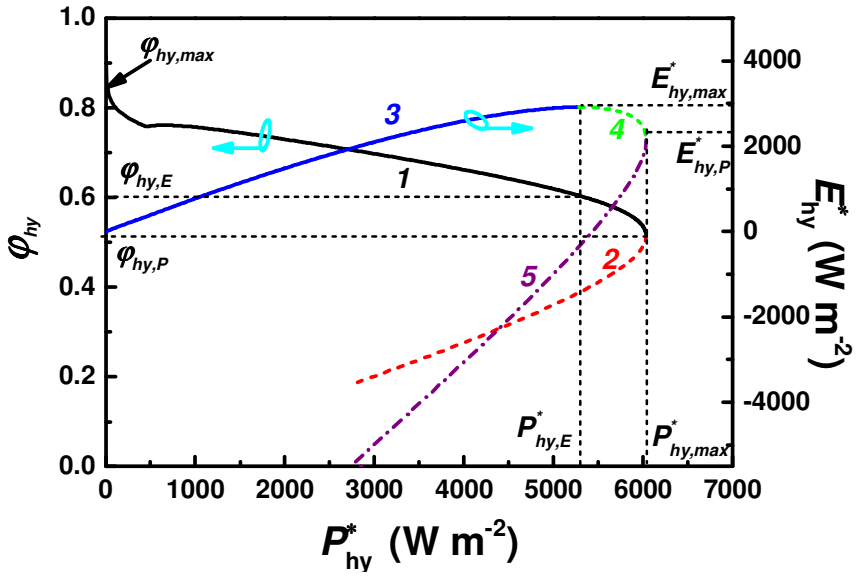

Fig. 7. Variations of φ_{hy} (curves 1 and 2) and E^*_{hy} (curves 3, 4 and 5) versus P^*_{hy}.

Fig. 8.

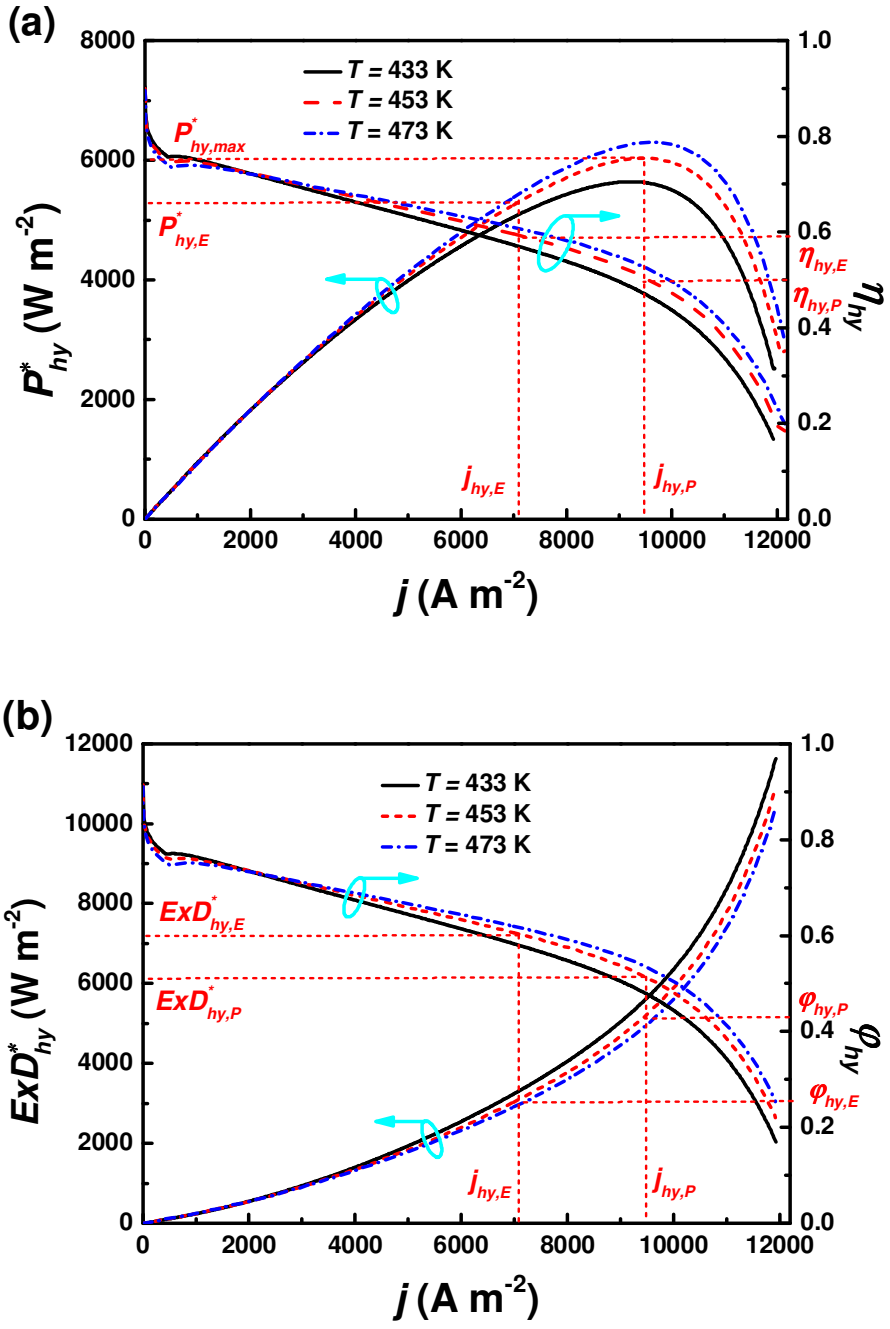
(a)
T = 433 K
T = 453 K
T = 473 K
P*hy,max
P*hy,E
ηhy,E
ηhy,P
jhy,E
jhy,P
P*hy (W m-2)
ηhy
j (A m-2)
(b)
T = 433 K
T = 453 K
T = 473 K
ExD*hy,E
ExD*hy,P
φhy,P
φhy,E
jhy,E
jhy,P
ExD*hy (W m-2)
φhy
j (A m-2)

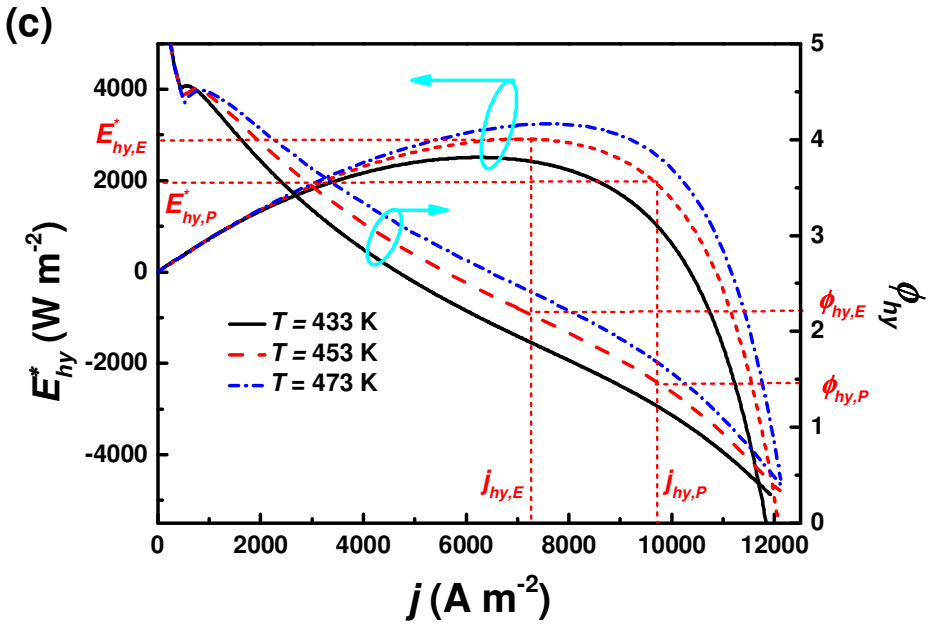

Fig. 8. Effects of the operating temperature T on (a) energetic, (b) exergetic and (c) ecological performances for the PAFC-ORC hybrid system.

Fig. 9.

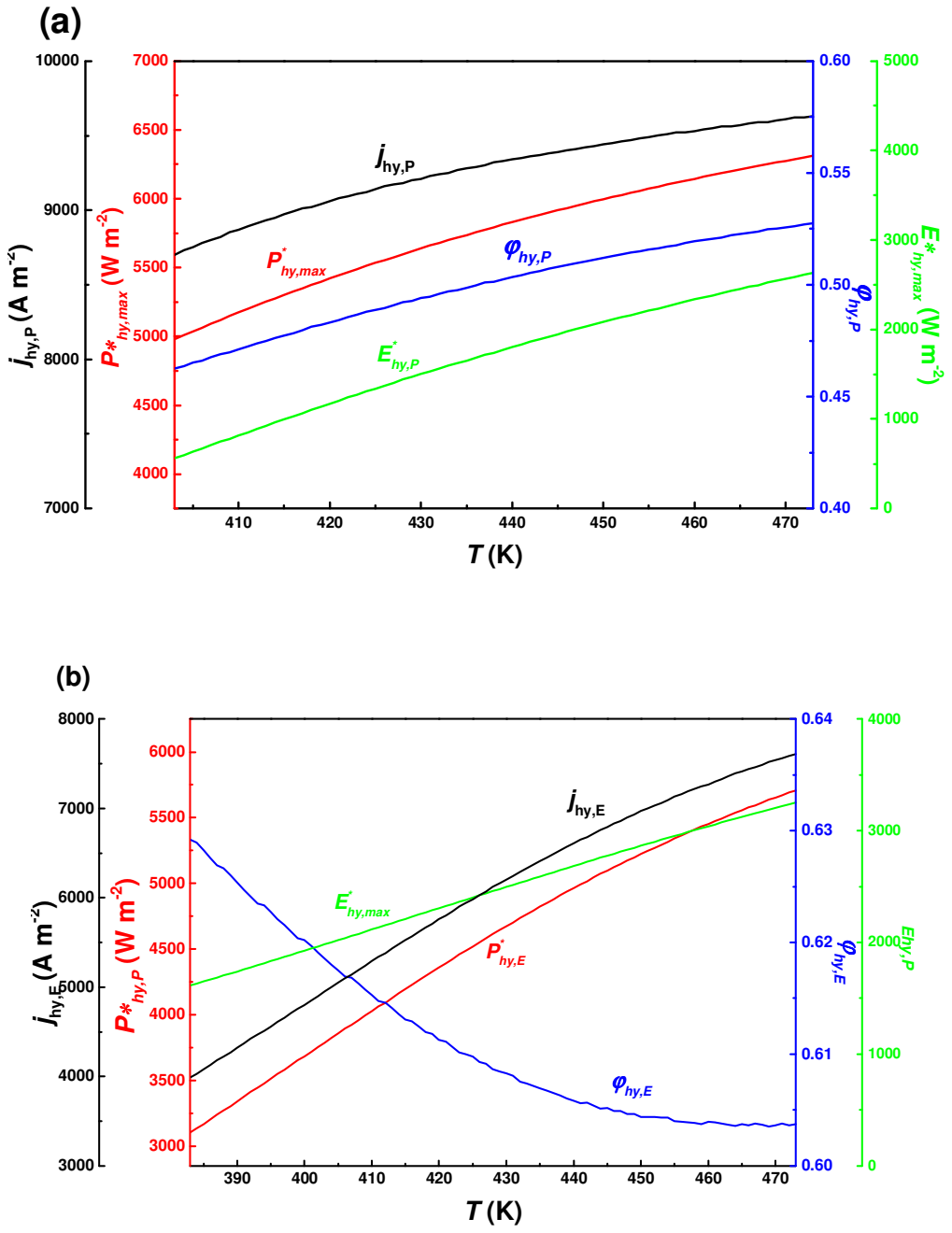

Fig. 9. (a) Variations of $j_{hy,P}$, $P^{*}_{hy,\max}$, $\varphi_{hy,P}$ and $E^{*}_{hy,P}$ versus T; and (b) Curves of $j_{hy,E}$, $P^{*}_{hy,E}$, $\varphi_{hy,E}$ and $E^{*}_{hy,\max}$ versus the operating temperature T.

Fig. 10.

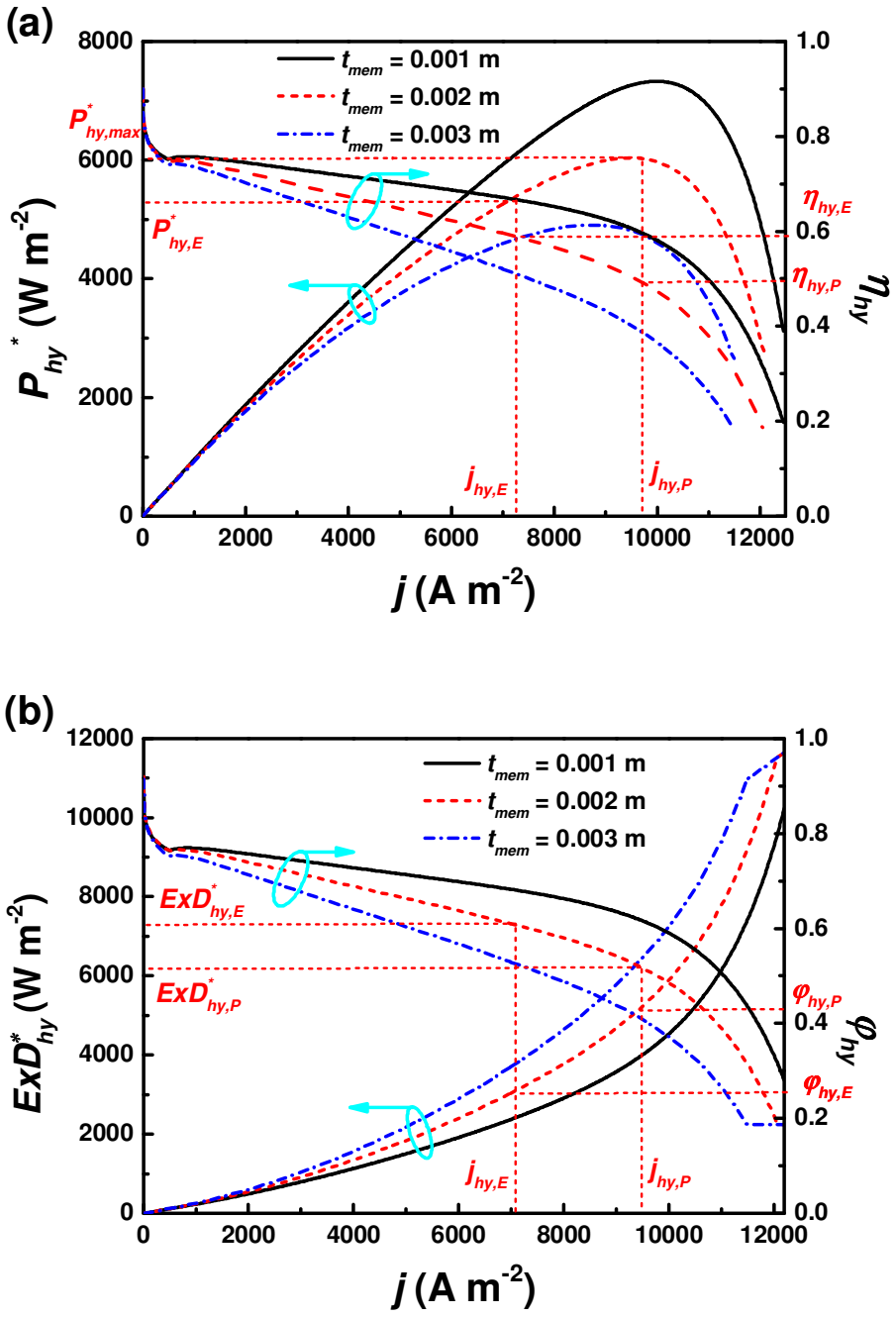
(a)
t_{mem} = 0.001 m
t_{mem} = 0.002 m
t_{mem} = 0.003 m
$P^*_{hy,max}$
$P^*_{hy,E}$
$\eta_{hy,E}$
$\eta_{hy,P}$
$j_{hy,E}$
$j_{hy,P}$
P^*_{hy} (W m^{-2})
η_{hy}
j (A m^{-2})
(b)
t_{mem} = 0.001 m
t_{mem} = 0.002 m
t_{mem} = 0.003 m
$ExD^*_{hy,E}$
$ExD^*_{hy,P}$
$\varphi_{hy,P}$
$\varphi_{hy,E}$
$j_{hy,E}$
$j_{hy,P}$
ExD^*_{hy} (W m^{-2})
ϕ_{hy}
j (A m^{-2})

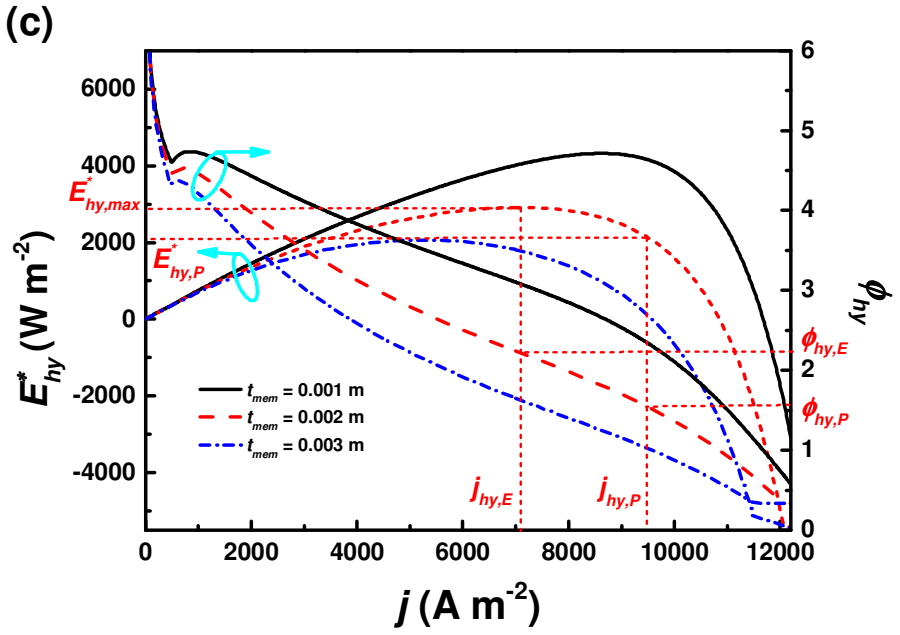

Fig. 10. Effects of the electrolyte thickness t_{ele} on (a) energetic, (b) exergetic and (c) ecological performances for the PAFC-ORC hybrid system.

Fig 11.

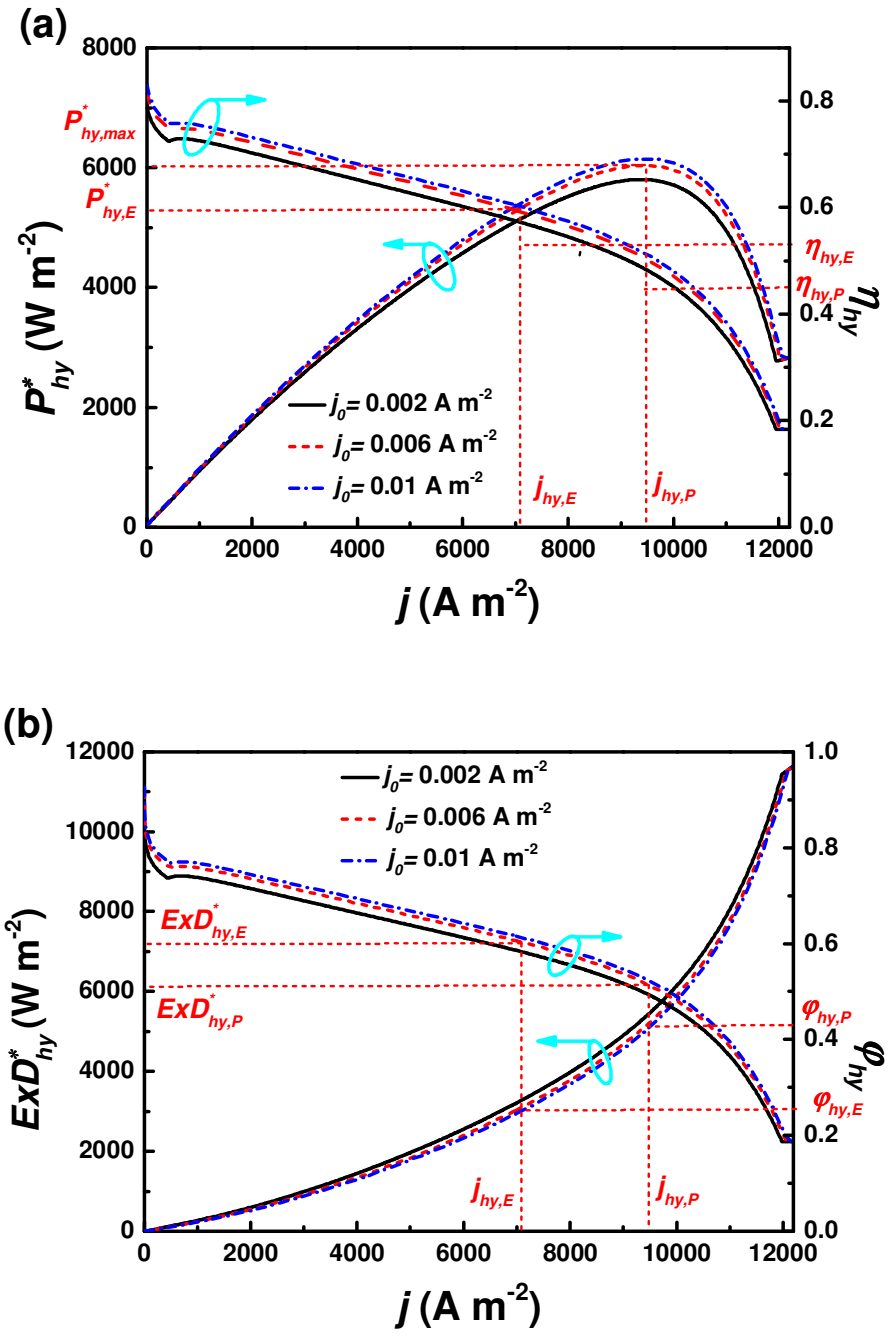
(a)
8000
6000
4000
2000
0
0.8
0.6
0.4
0.2
0.0
0
2000
4000
6000
8000
10000
12000
$P^*_{hy,max}$
$P^*_{hy,E}$
P^*_{hy} (W m^{-2})
η_{hy}
$\eta_{hy,E}$
$\eta_{hy,P}$
j_0= 0.002 A m^{-2}
j_0= 0.006 A m^{-2}
j_0= 0.01 A m^{-2}
$j_{hy,E}$
$j_{hy,P}$
j (A m^{-2})
(b)
12000
10000
8000
6000
4000
2000
0
1.0
0.8
0.6
0.4
0.2
0.0
$ExD^*_{hy,E}$
$ExD^*_{hy,P}$
ExD^*_{hy} (W m^{-2})
φ_{hy}
$\varphi_{hy,P}$
$\varphi_{hy,E}$
j_0= 0.002 A m^{-2}
j_0= 0.006 A m^{-2}
j_0= 0.01 A m^{-2}
$j_{hy,E}$
$j_{hy,P}$
j (A m^{-2})

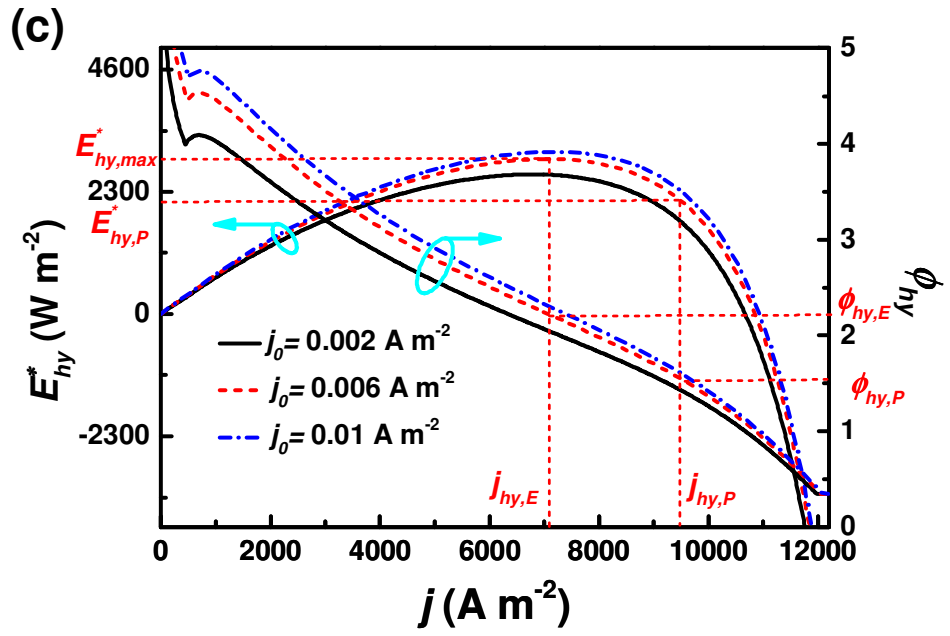

Fig. 11. Effects of the exchange current density j_0 on (a) energetic, (b) exergetic and (c) ecological performances for the PAFC-ORC hybrid system.

Fig. 12.

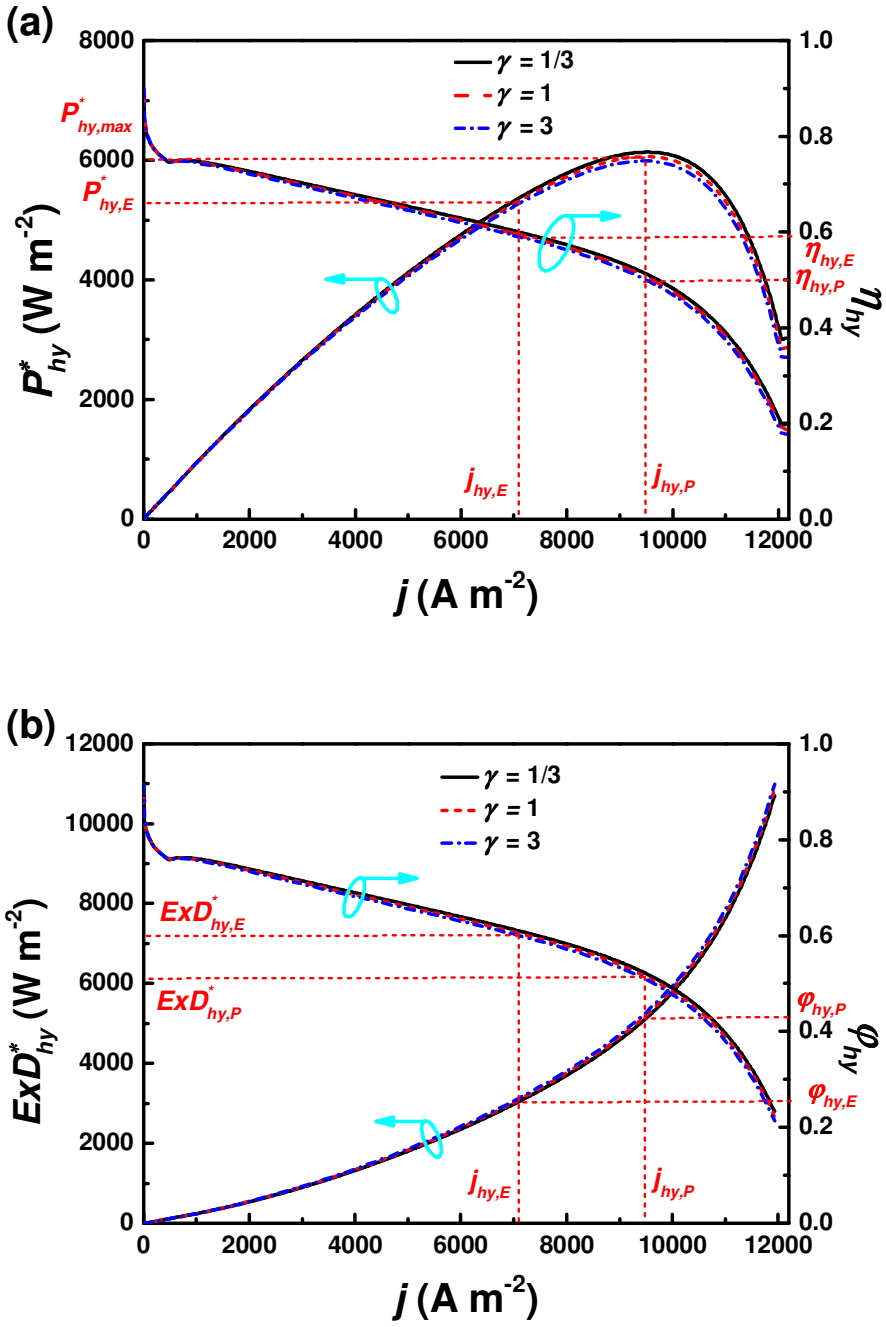
(a)
γ = 1/3
γ = 1
γ = 3
P*hy,max
P*hy,E
P*hy (W m-2)
ηhy
ηhy,E
ηhy,P
jhy,E
jhy,P
j (A m-2)
(b)
γ = 1/3
γ = 1
γ = 3
ExD*hy,E
ExD*hy,P
ExD*hy (W m-2)
φhy
φhy,P
φhy,E
jhy,E
jhy,P
j (A m-2)

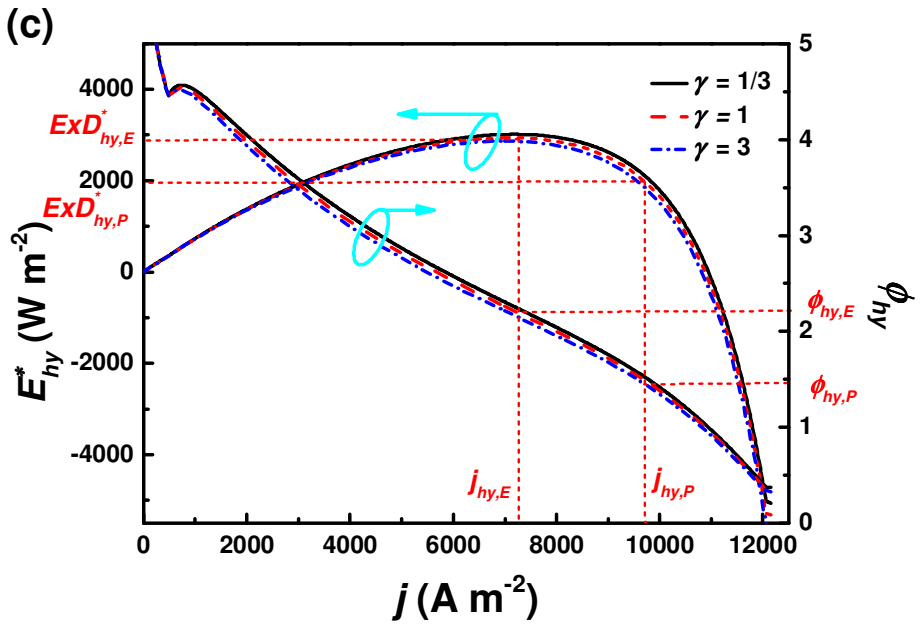

Fig. 12. Effects of the pinch temperature ratio γ on (a) energetic, (b) exergetic and (c) ecological performances for the PAFC-ORC hybrid system.

Fig. 13.

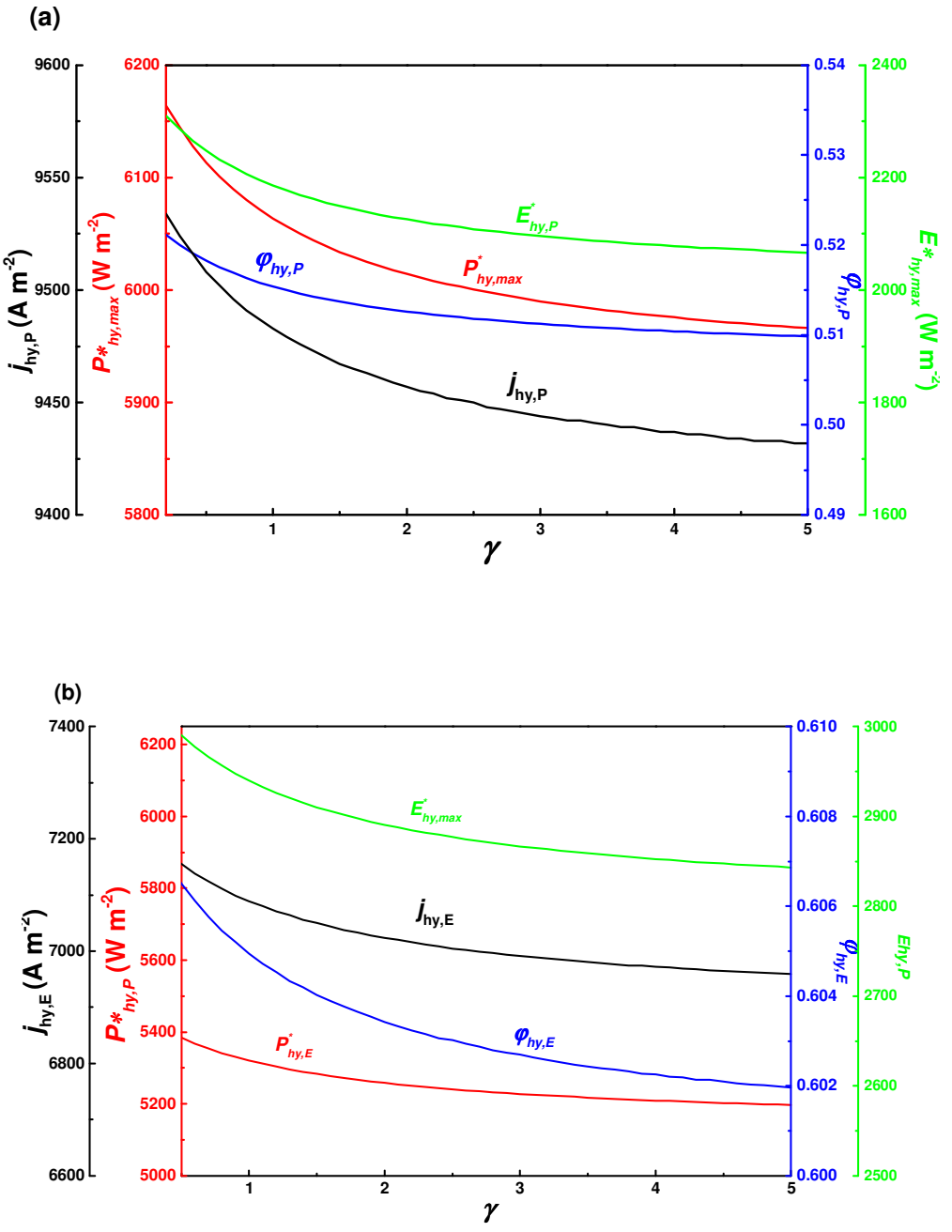

Fig. 13. (a) Variations of $j_{hy,P}$, $P^*_{hy,\max}$, $\varphi_{hy,P}$ and $E^*_{hy,P}$ versus the pinch temperature ratio γ; and (b) Curves of $j_{hy,E}$, $P^*_{hy,E}$, $\varphi_{hy,E}$ and $E^*_{hy,\max}$ versus the pinch temperature ratio γ.